Electronic Supplementary Material (ESI) for New Journal of Chemistry.

Revisiting the fluoride binding behaviour of Dipyrrolylquinoxaline in aqueous medium: a Copper ion mediated approach

Supplementary Information

Rituraj Das,[a] Plaban J Sarma,[a] Abhishek Borborah,[a] Sudhangshu P Bharati[a] and Sanjeev P Mahanta[a*]

[a]Department of Chemical Sciences, Tezpur University, Tezpur, Assam, India.

Email: spm@tezu.ernet.in; samahanta@gmail.com

General Methods

Instrumentation and reagents: All reagents and solvents were obtained from commercial sources and used as received, without further purification. All tetrabutylammonium salts for anion screening experiments were purchased from Sigma-Aldrich® and used as such. Infrared and Far-IR spectra were recorded with a Perkin Elmer Frontier MIRFIR spectrometer.

The electrospray ionization mass spectrometry (ESI-MS) spectrum of the receptor was recorded in acetonitrile in Shimadzu-LCMS-2010 mass spectrometer. The ^{1}H NMR spectra (400 MHz), ^{13}C NMR spectra (100 MHz) and ^{19}F NMR spectra were recorded on a 'JEOL' NMR spectrophotometer in DMSO-d_6 and chloroform-d_1 at room temperature. In NMR spectra, chemical shifts are reported in parts per million (ppm) downfield of Me_4Si (TMS) as internal standard. EPR analysis was carried out with JEOL, Model: JES-FA200 spectrometer.

Cyclic Voltammogram analysis was performed with CHI660A Potentiostate, whereas the Differential Pulse Voltammetry (DPV) was done using Bio-Logics SP-300 with EIS facility. UV-Vis experiments were performed with Shimadzu UV-2550 spectrophotometer. UV-Vis titrations were carried out in chloroform and dimethyl sulfoxide solution. The receptor solutions were titrated by adding known quantities of concentrated solution of the anions in question. Cyclic voltammetry experiments were carried out in a standard three electrode apparatus with a platinum working electrode, Ag/AgCl as reference electrode, and a Pt wire auxiliary electrode. The supporting electrolyte is 0.1 M tetrabutylammonium perchlorate (TBAP) in DMSO solution. The cell was maintained oxygen-free by passing dry nitrogen through the solution.

The limit of blank (LoB) and limit of detection (LoD) are calculated from the replicates of a blank sample and absorption calibration curves respectively.[1]

LoB is estimated by measuring replicates of a blank sample and calculating the mean result and the standard deviation (SD).

$$LoB = \text{mean blank} + 1.645(SD_{blank})$$

LoD is determined by utilizing both the measured LoB and test replicates of a sample known to contain a low concentration of analyte. The mean and SD of the low concentration sample is then calculated according to

$LoD = LoB + 1.645(SD_{low\ concentration\ sample})$

Demonstration of Fluoride Ion Sensing in Toothpastes and real life samples: For the detection of F^- ion in toothpastes, 268 mg of Sensodyne toothpaste (gsk) was extracted separately in 2 mL aqueous DMSO and the resulting suspension was filtered to obtain colorless clear solution (Toothpaste extract, **TE**).

The fluoride contaminated water samples collected from Baghpani village, Karbi Anglong, Assam, India was used as such.

Computational details

To explore the structure, stability and the properties of the complex, we have performed density functional theory (DFT) calculations using Gaussian09 software package.[2] Geometry relaxation along with the frequency and natural bond orbital (NBO)[3] calculation is carried out at wB97XD/SDD/def2tzv[4,5] level of theory employing ultrafine integration grid and Grimme's D2 dispersion correction to bring accuracy into the calculation. The solvent effect was counted by using CPCM method available in the Gaussian09 software suite. On the other hand, NBO analysis helps us to understand the nature of interaction between the Cu and the ligands as well as also to locate their interacting molecular orbitals. Finally, to support the experimental data, time dependent density functional theory (TD-DFT)[6] calculation is done to predict the exited state properties of the complex implementing the same level of theory.

Synthesis and characterization

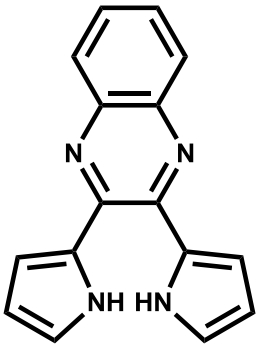

SR1

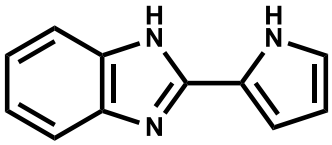

SR2

Figure S1: Structure of the receptors **SR1** and **SR2** chosen for the study.

A. Synthesis of 2,3-dipyrrol-2′-ylquinoxaline (SR1)

2, 3-dipyrrol-2′-ylquinoxaline was prepared according to literature reported procedure.[7] Briefly, 2, 3-dipyrrol-2′-yl-ethanedione (5.3 mmol) was prepared and dissolved in glacial acetic acid (50 mL) and to this solution was added *ortho*-phenylenediamine (11.5 mmol) in acetic acid (30 mL) with stirring. The resultant mixture was refluxed for 90 min. After this 100 mL of water was added to the reaction mixture followed by dichloromethane. The organic phase was separated off and the aqueous phase was further extracted with dichloromethane. The organic phases were combined and washed with saturated aqueous sodium bicarbonate solution, water, and brine. After drying over anhydrous sodium sulfate, the solution was evaporated to dryness and separated using silica gel column chromatography (Ethyl acetate/hexane eluent, 10%) to afford **SR1** as greenish yellow powder. ^{1}H NMR (400MHz, DMSO-d_6) δ 6.10 (m, 2H), 6.21 (m, 2H), 6.95 (m, 2H), 7.66 (dd, 2H), 7.91 (dd, 2H), 11.54 (br s, 2H); ^{13}C NMR (100MHz, DMSO-d_6) δ 109.4, 112.1, 121.9, 128.5, 129.2, 129.6, 139.9, 145.5; LCMS m/z calculated for $C_{16}H_{12}N_4$ [M + H]: 261.11 found: 261.11; UV-Vis (DMSO) λ_{max} (nm): 262, 300, 404.

B. Synthesis of Bis(pyrrole-benzimidazole) (SR2)

Bis(pyrrole-benzimidazole) was prepared according to literature reported procedure.[8] To a solution of *ortho*-phenylenediamine (1 mmol) in nitrobenzene, pyrrole-2-carboxaldehyde (1 mmol) was added. The reaction mixture was heated at 120°C for 24 h. The precipitated solid was filtered, washed with first hexane and then diethyl ether and purified by column chromatography on silica gel with 1% MeOH in $CHCl_3$ as eluent. Subsequently, the product was recrystallized from 1:1 acetone and methanol mixture. ^{1}H-NMR (400 MHz, DMSO-d_6): δ 12.48 (s, 1H, NH), 11.79 (s, 1H), 7.48 (d, br, 2H), 7.12 (q, 2H, CH, 2.88 Hz), 6.92 (m, 1H), 6.84 (m, 1H), 6.19 (m, 1H).^{13}C-NMR (100 MHz, DMSO-d_6) δ 147.2, 123.1, 121.8, 121.7, 109.6, 109.5. LCMS m/z calculated for $C_{11}H_9N_3$ (M+H) 184.08, found 184.08; UV-Vis (DMSO) λ_{max} (nm): 312, 327.

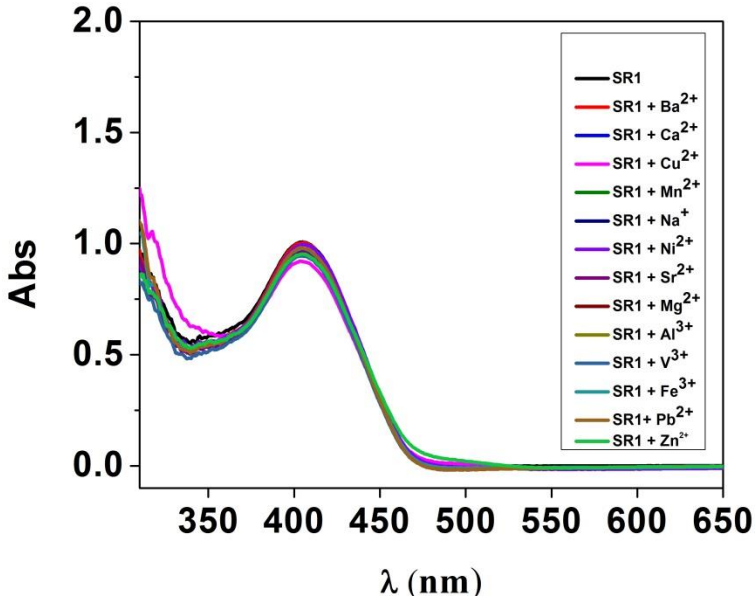

Figure S2: Change in the UV-Vis spectra of **SR1** (68 x 10^{-6} M) in DMSO solution upon addition of different metal salts ($BaSO_4$, $CaCO_3$, $CuCl_2$, $MnCl_2$, NaCl, $NiSO_4.6H_2O$, $SrCl_2$, $MgSO_4$, $AlCl_3$, VCl_3, $FeSO_4$, $PbSO_4$, $ZnCl_2$) as aqueous solution.

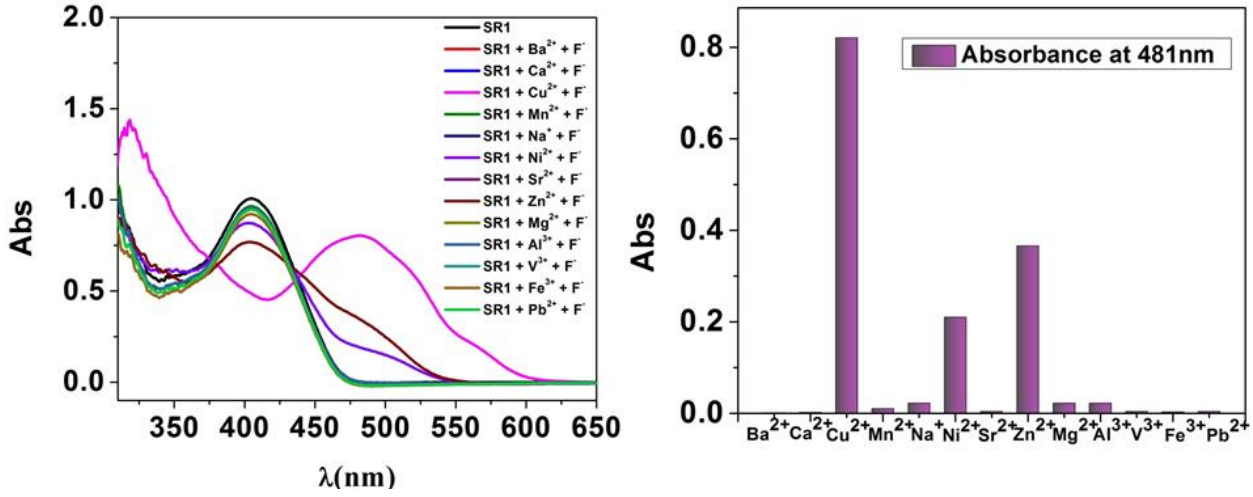

Figure S3 left**:** Change in the UV-Vis spectra of **SR1:M^{n+}** ([**SR1**] = 68 x 10^{-6} M and M^{n+} = 25 x 10^{-3} M) in DMSO/water mixture upon addition fluoride to the respective **SR1:M^{n+}** system where M^{n+} = Ba^{2+}, Ca^{2+}, Cu^{2+}, Mn^{2+}, Na^{+}, Ni^{2+}, Sr^{2+}, Zn^{2+}, Mg^{2+}, Al^{3+}, V^{3+}, Fe^{2+}, Pb^{2+}as aqueous solution; right: bar diagram corresponding to the absorbance at 481nm in presence of different metal ions screened.

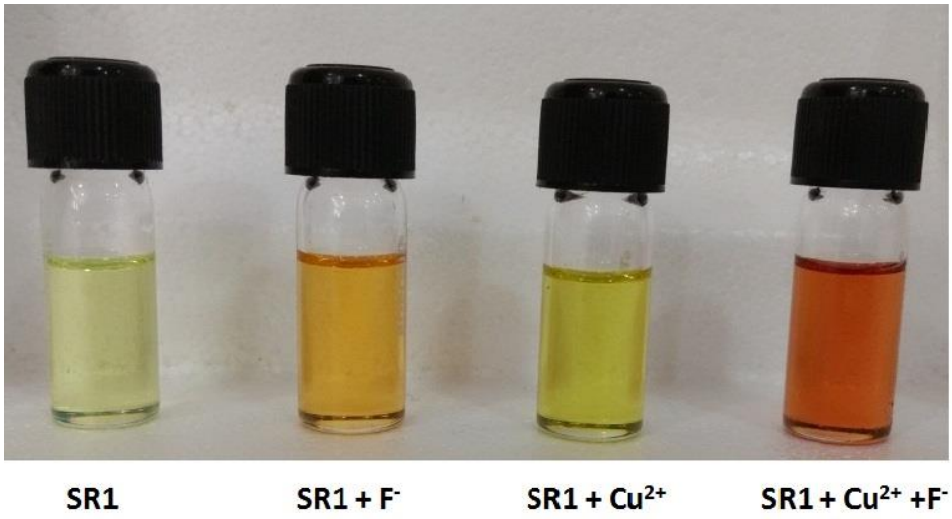

Figure S4: Change in the colour of **SR1** solution upon addition of F^- and sequential addition of aqueous $CuCl_2$ and TBAF in DMSO.

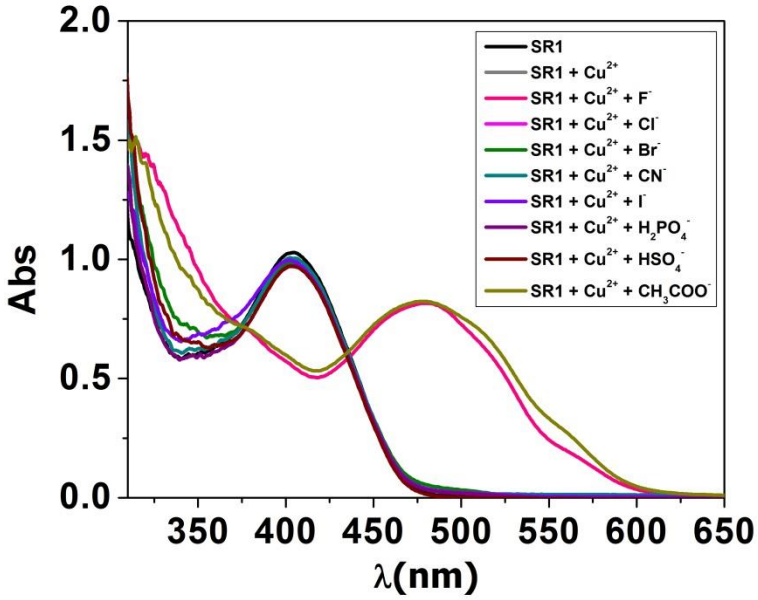

Figure S5: Change in the UV-Vis spectra of **SR1** solution ([**SR1**] =68 x 10^{-6} M) in DMSO upon sequential addition of aqueous $CuCl_2$ ([Cu^{2+}] = 2.5 x 10^{-3} M) solution and different anions (F^-, Cl^-, Br^-, CN^-, I^-, $H_2PO_4^-$, HSO_4^-, CH_3COO^-) as their tetrabutylammonium salt in DMSO.

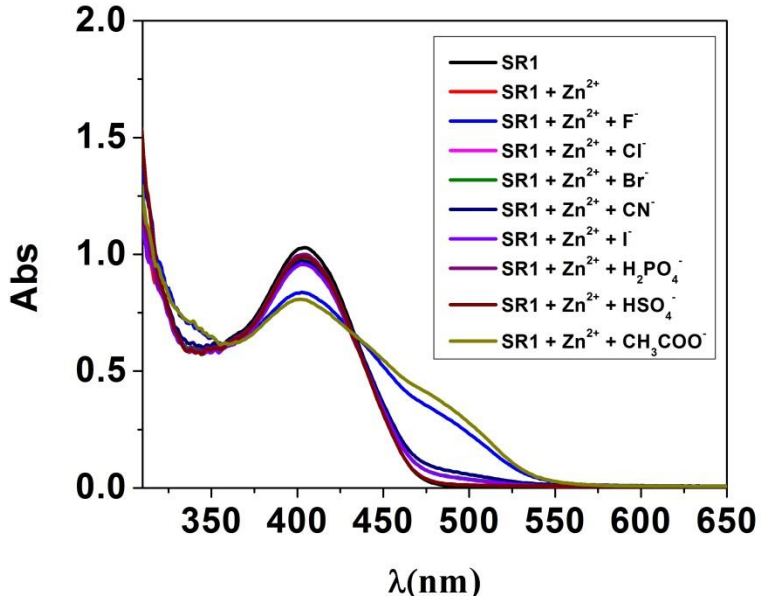

Figure S6: Change in the UV-Vis spectra of **SR1** solution ([**SR1**] =68 x 10^{-6} M) in DMSO upon sequential addition of aqueous $ZnCl_2$ ([Zn^{2+}] =25 x 10^{-3} M) solution and different anions (F^-, Cl^-, Br^-, CN^-, I^-, $H_2PO_4^-$, HSO_4^-, CH_3COO^-,) as their tetrabutylammonium salt in DMSO.

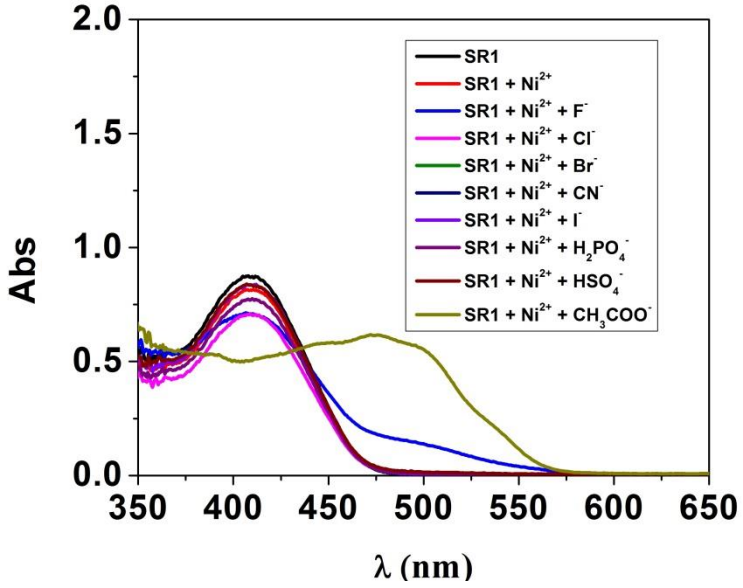

Figure S7: Change in the UV-Vis spectra of **SR1** solution ([**SR1**] =68 x 10^{-6} M) in DMSO upon sequential addition of aqueous ([Ni^{2+}] =25 x 10^{-3} M) solution and different anions (F^-, Cl^-, Br^-, CN^-, I^-, $H_2PO_4^-$, HSO_4^-, CH_3COO^-,) as their tetrabutylammonium salt in DMSO.

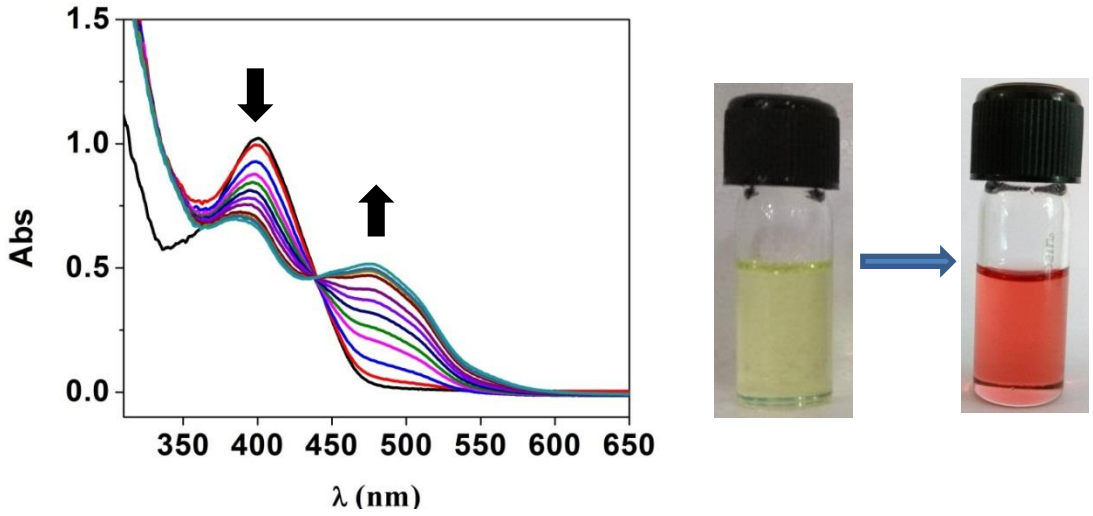

Figure S8 left: Evolution of UV-Vis spectra of **SR1** and Cu^{2+} ([**SR1**] = 68 x 10^{-6} M, [Cu^{2+}] = 15.4 x 10^{-5} M) mixture in DMSO/water upon gradual addition of F^- ion (50 x 10^{-3}M) in DMSO; right: picture of red coloured solution upon successive addition of F^- ion to the **SR1** and Cu^{2+} mixture.

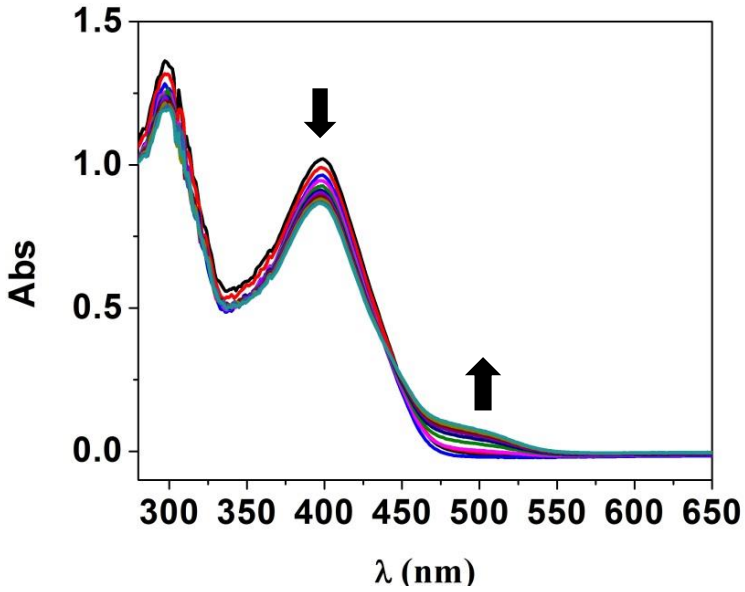

Figure S9: Evolution of UV-Vis spectra of **SR1** and F^- ([**SR1**] = 68 x 10^{-6} M, [F^-] = 6 x 10^{-4} M) mixture in DMSO upon gradual addition of aqueous $CuCl_2$ solution (25 x 10^{-3} M).

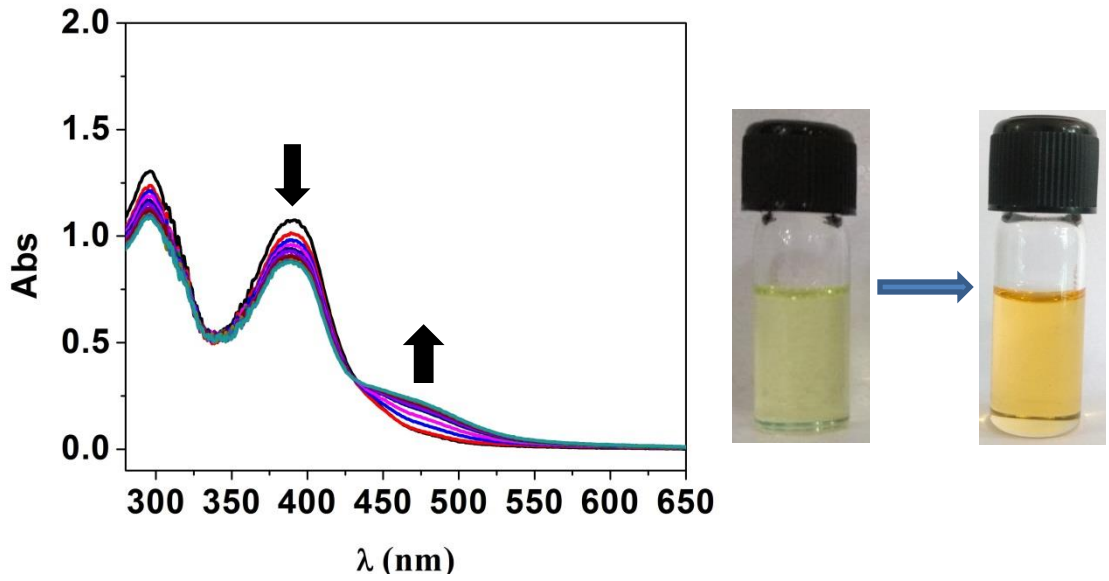

Figure S10 left: Evolution of UV-Vis spectra of **SR1** and Zn^{2+} ([**SR1**] =68 x 10^{-6} M, [Zn^{2+}] = 15.4 x 10^{-5} M) mixture in DMSO/water upon gradual addition of F^- ion (50 x 10^{-3}M) in DMSO; right: picture of orange coloured solution upon successive addition of F^- ion to the **SR1** and Zn^{2+} mixture.

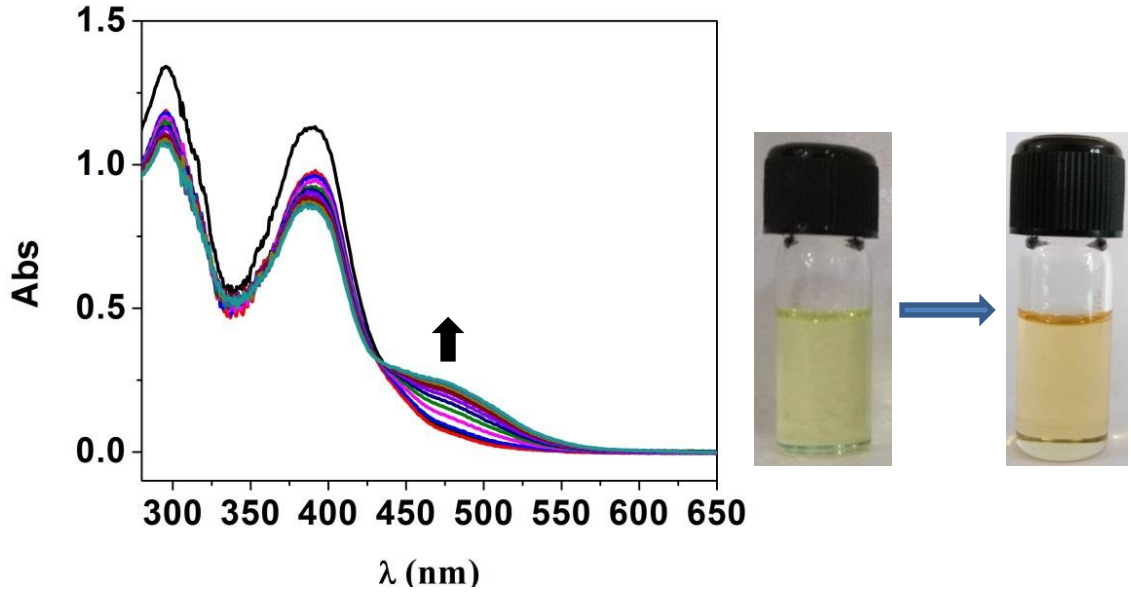

Figure S11 left: Evolution of UV-Vis spectra of **SR1** and Ni^{2+} ([**SR1**] = 68 x 10^{-6} M, [Ni^{2+}] = 15.4 x 10^{-5} M) mixture in DMSO/water upon gradual addition of F^- ion (50 x 10^{-3}M) in DMSO; right: picture of light orange coloured solution upon successive addition of F^- ion to the **SR1** and Ni^{2+} mixture.

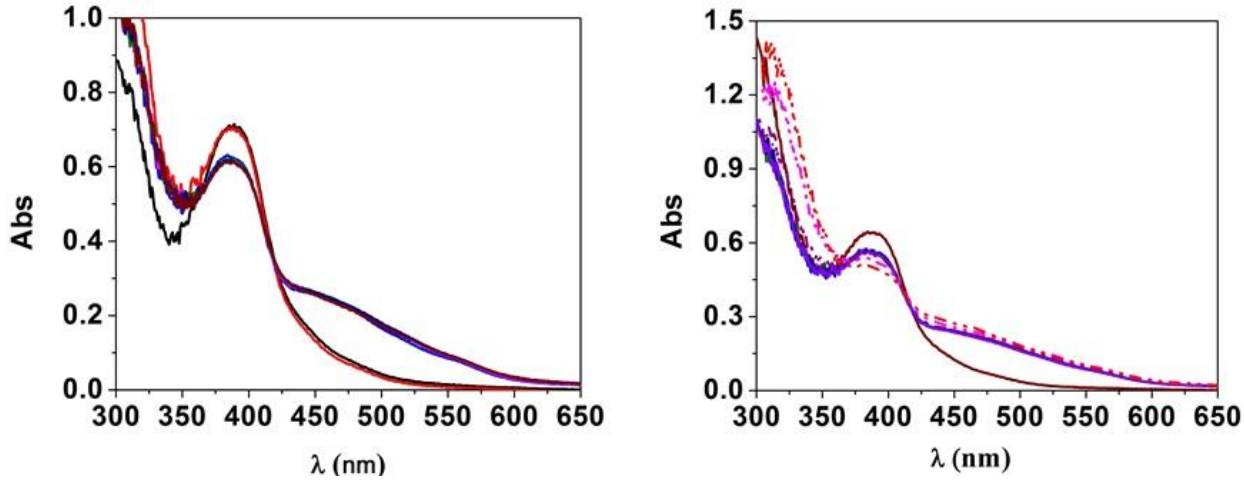

Figure S12 left: UV-Vis spectra of **SR1** and Cu^{2+} ([**SR1**] = 68 x 10^{-6} M, [Cu^{2+}] = 15.4 x 10^{-5} M) mixture in DMSO/water upon gradual addition (20-200µl) of CH_3COO^- ion (50 x 10^{-3}M) in DMSO; right: UV-Vis spectra of **SR1** and Cu^{2+} mixtures after addition of F^- (dotted lines) in presence CH_3COO^- (200µl) ions in DMSO/Water mixture.

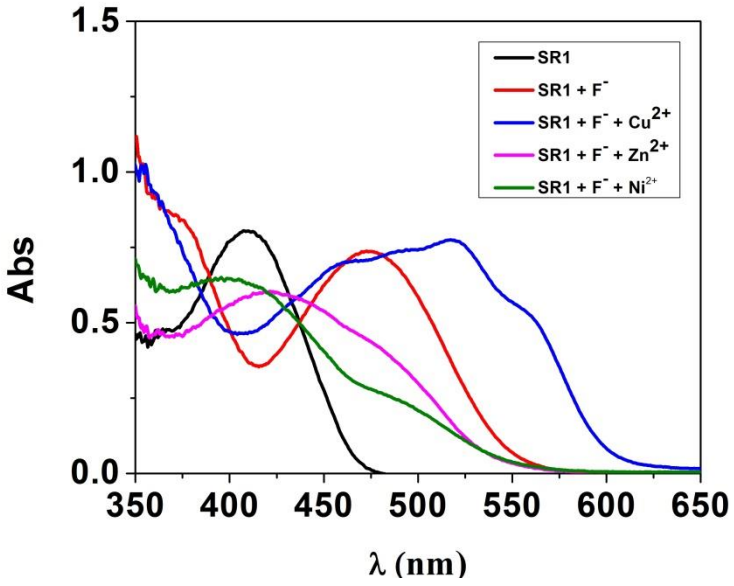

Figure S13: Change in the UV-Vis spectra of **SR1.F**$^-$ ([**SR1**] = 68 x 10^{-6} M and F^- = 15 x 10^{-4} M) in DMSO upon sequential addition $CuCl_2$, $ZnCl_2$, $NiSO_4.6H_2O$ as aqueous solution.

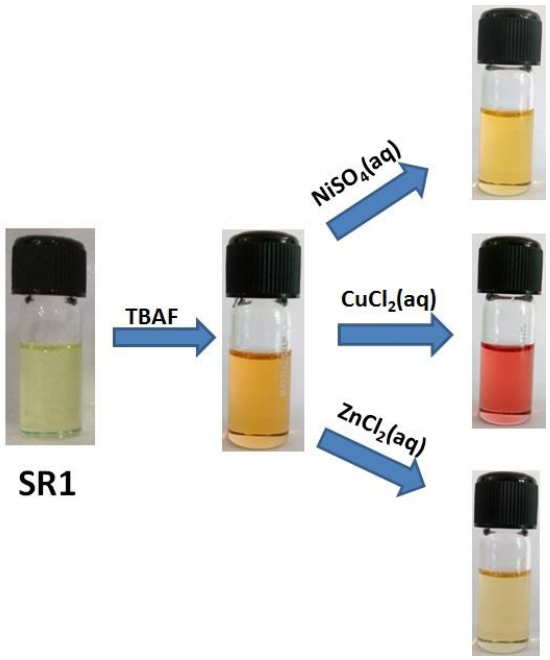

Figure S14: Schematic representation of the colorimetric change upon addition of aqueous solution of $CuCl_2$, $ZnCl_2$ and $NiSO_4.6H_2O$ of same concentration 15.4 x 10^{-5}M to the **SR1**.F^- complex in DMSO.

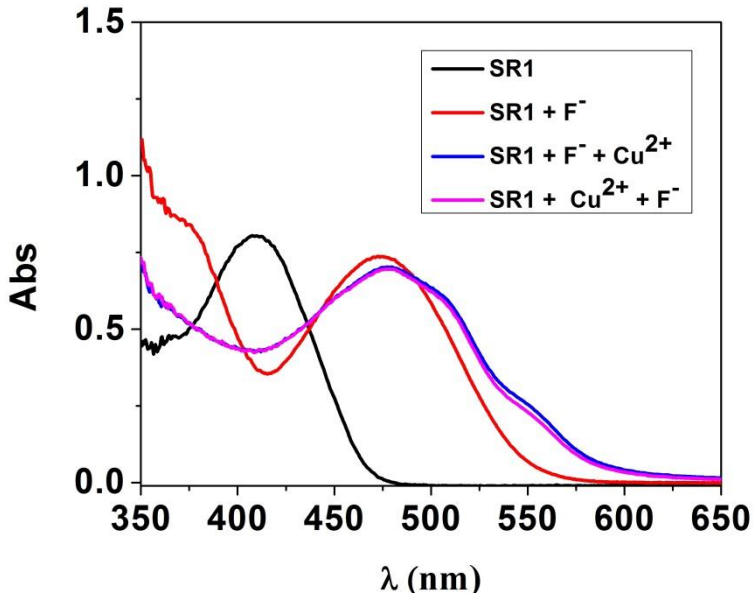

Figure S15: UV-Vis spectra of **SR1** after addition of F^- (red) in DMSO, sequential addition of F^- and Cu^{2+} (blue) and addition in reverse order of Cu^{2+} and F^-(pink) in DMSO/Water mixture.

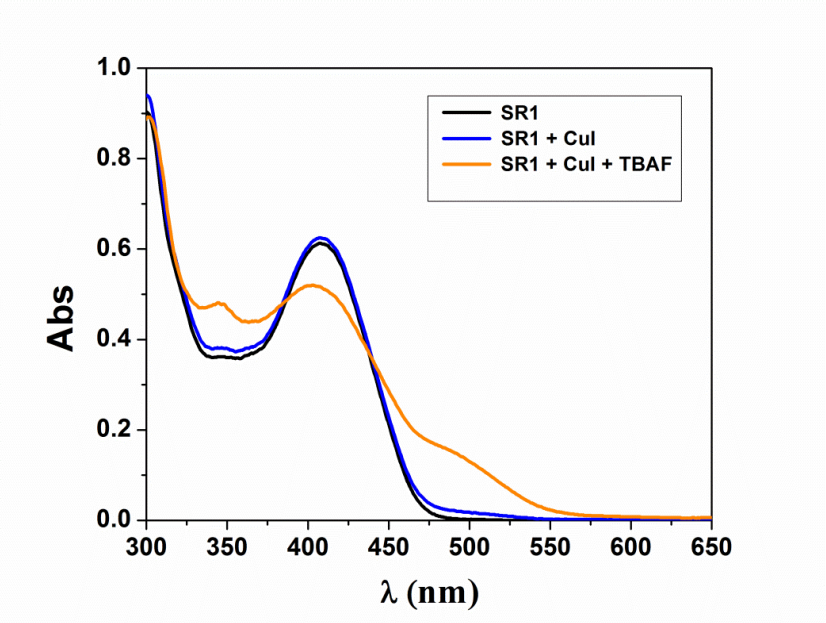

Figure S16: UV-Vis spectra of **SR1** after addition of Cu(I) salt and TBAF in DMSO/Water mixture.

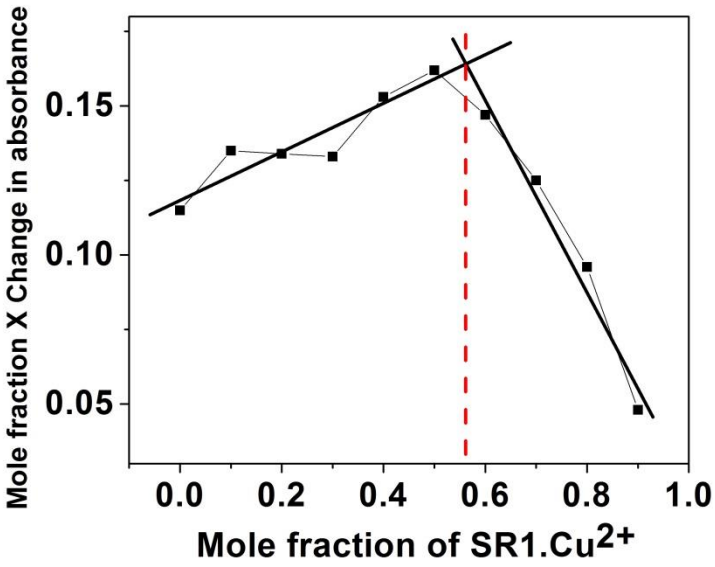

Figure S17: Job's plot for **SR1**.Cu^{2+} ([**SR1**] = 11 x 10^{-5} M, [Cu^{2+}] = 11 x 10^{-5} M) DMSO/water mixture and F^- (11`x 10^{-5} M) in DMSO.

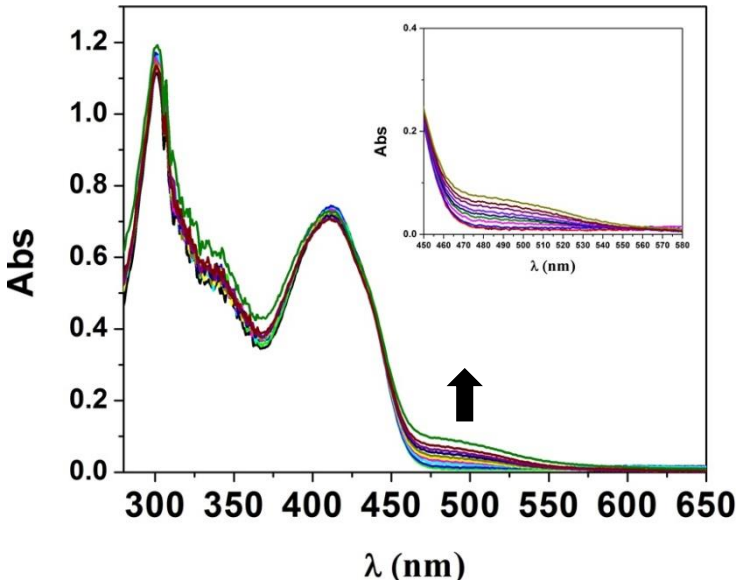

Figure S18: Evolution of UV-Vis spectra of **SR1** and Cu^{2+} ([**SR1**] = 66 x 10^{-6} M, [Cu^{2+}] = 15.5 x 10^{-3} M) mixture in $CHCl_3$/water medium upon gradual addition of F^- ion (50 x 10^{-3}M) in $CHCl_3$. Inset: Expanded region for the new band on gradual addition of F^-.

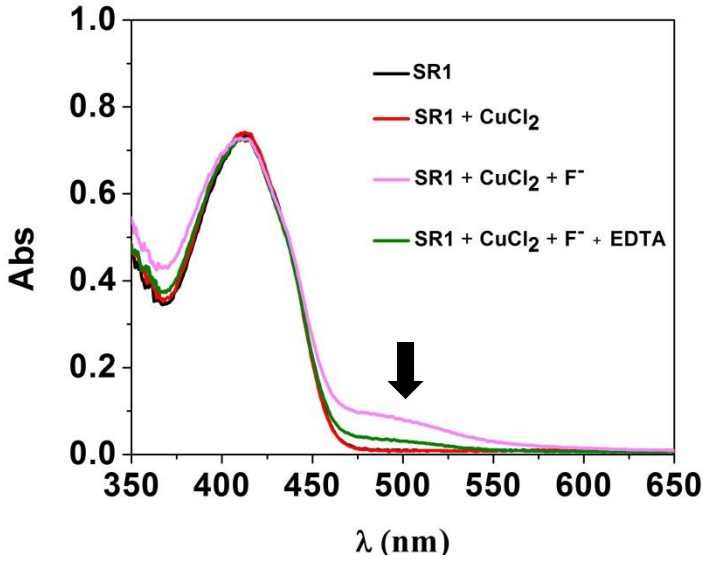

Figure S19: Change in the UV-Vis spectra of the **SR1 + Cu^{2+}+ F^-** red coloured solution after gradual addition of EDTA in water to the $CHCl_3$/water mixture.

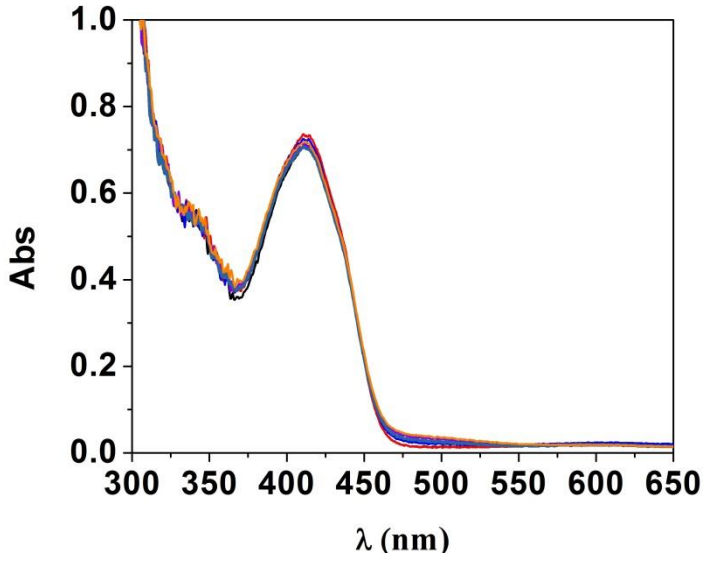

Figure S20: UV-Vis spectra of **SR1** and Cu^{2+} ([**SR1**] = 66 x 10^{-6} M, [Cu^{2+}] = 15.5 x 10^{-3} M) mixture in $CHCl_3$/water medium upon gradual addition of CH_3COO^- ion (50 x 10^{-3}M) in $CHCl_3$.

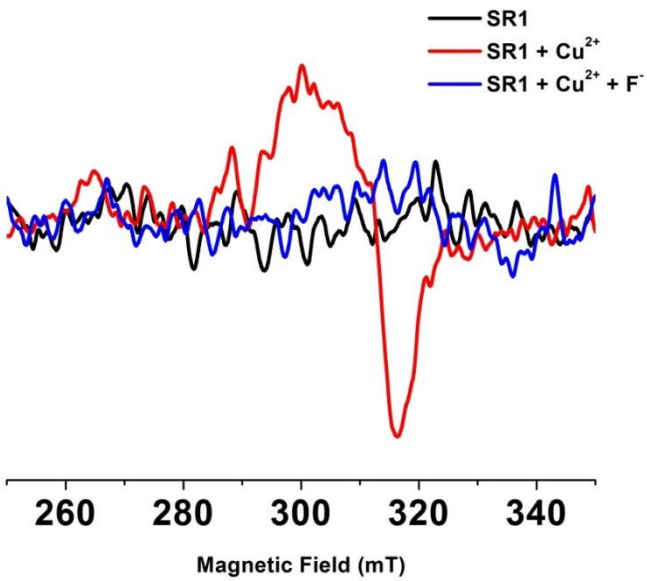

Figure S21: EPR spectra (100K, DMSO) [red: addition of $CuCl_2$ (aq) to **SR1** solution; blue: addition of $CuCl_2$(aq) to **SR1** solution followed by NaF (aq).

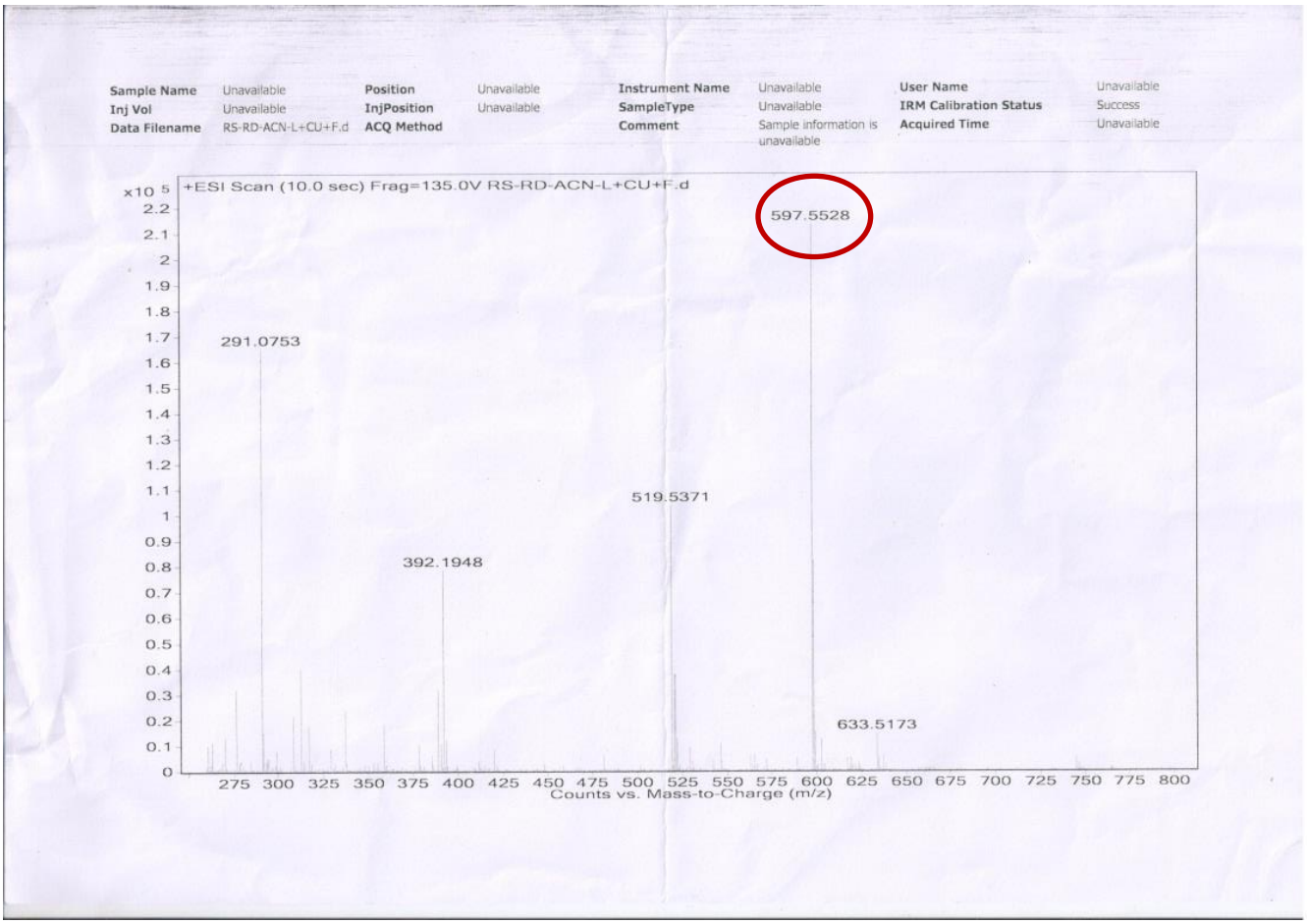

Figure S22: LCMS spectrum of the complex $[Cu(\mathbf{SR1})_2OH]^{2-}$.

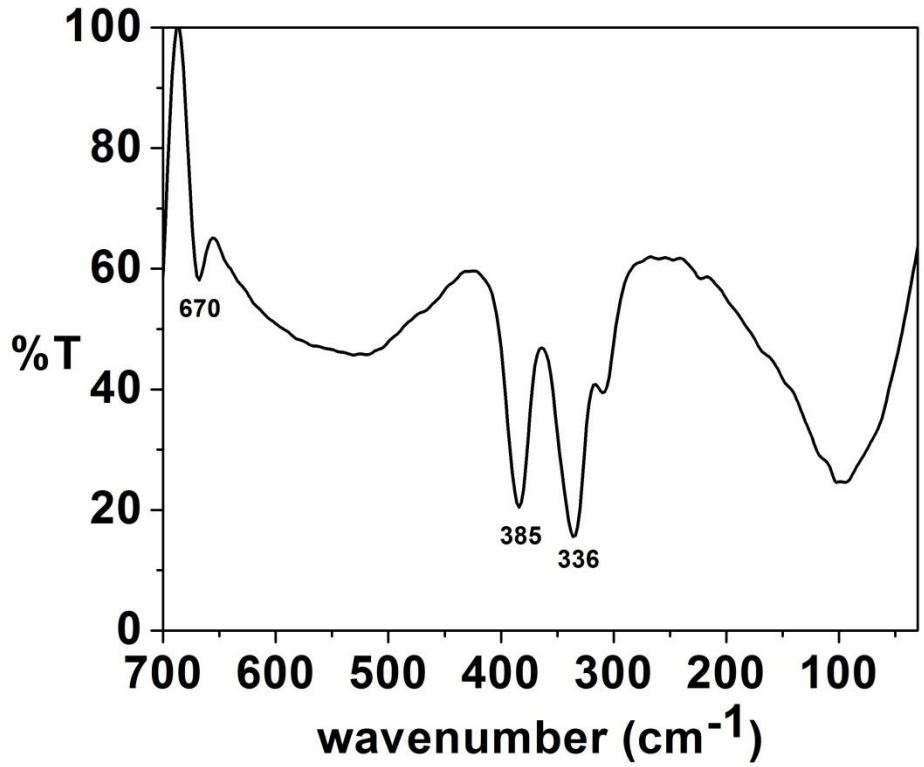

Figure S23: Far-IR spectrum of the red coloured solution obtained after sequential addition of $CuCl_2$ and TBAF in **SR1** solution in DMSO $[Cu(\mathbf{SR1})_2OH]^{2-}$.

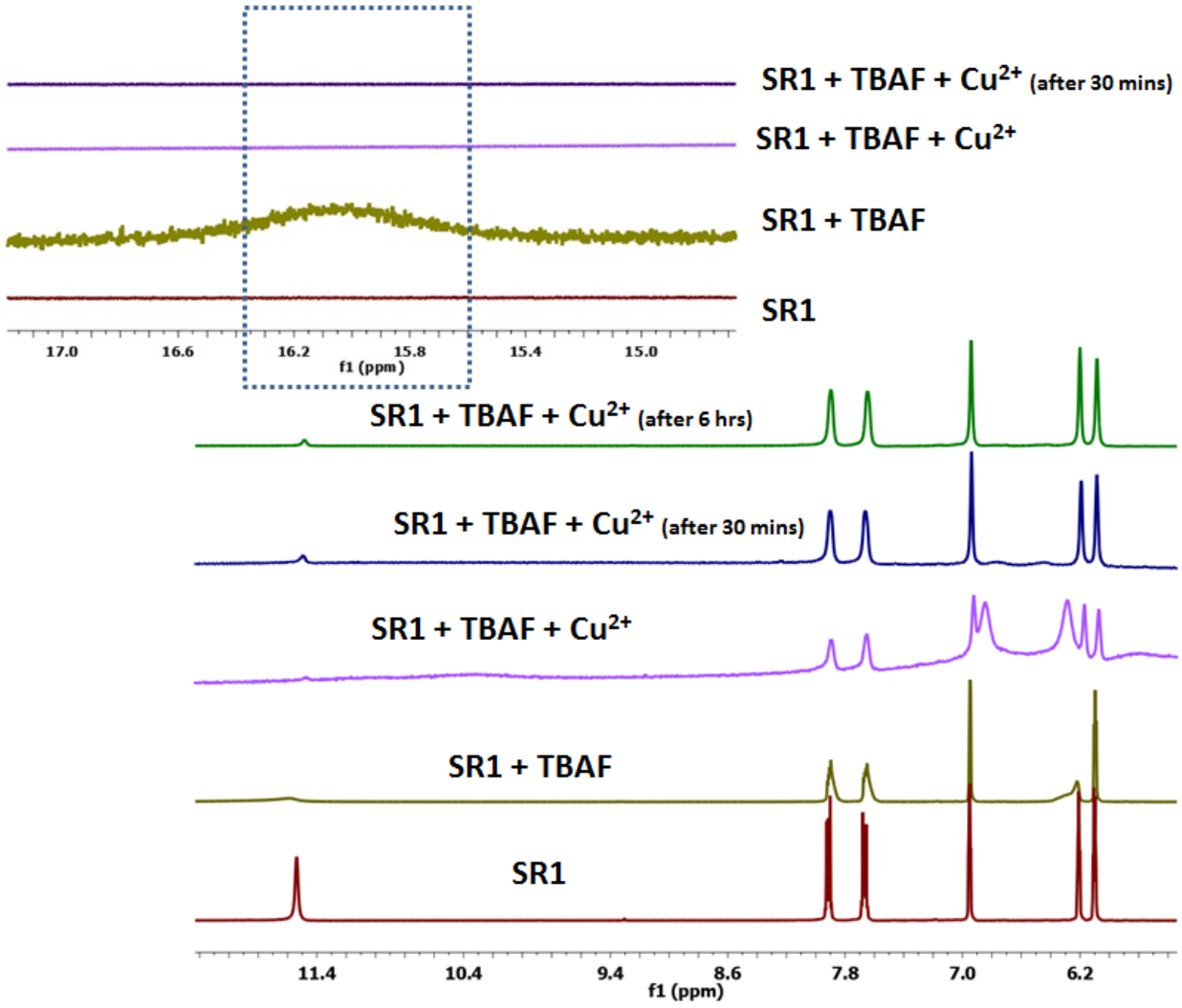

Figure S24: ^{1}H NMR spectra of **SR1** in DMSO-d_6 upon sequential addition of F^- followed by $CuCl_2$ in D_2O with time.in DMSO/D_2O mixture. Inset: expanded region around 16 ppm to confirm the appearance peak corresponding to HF_2^-.

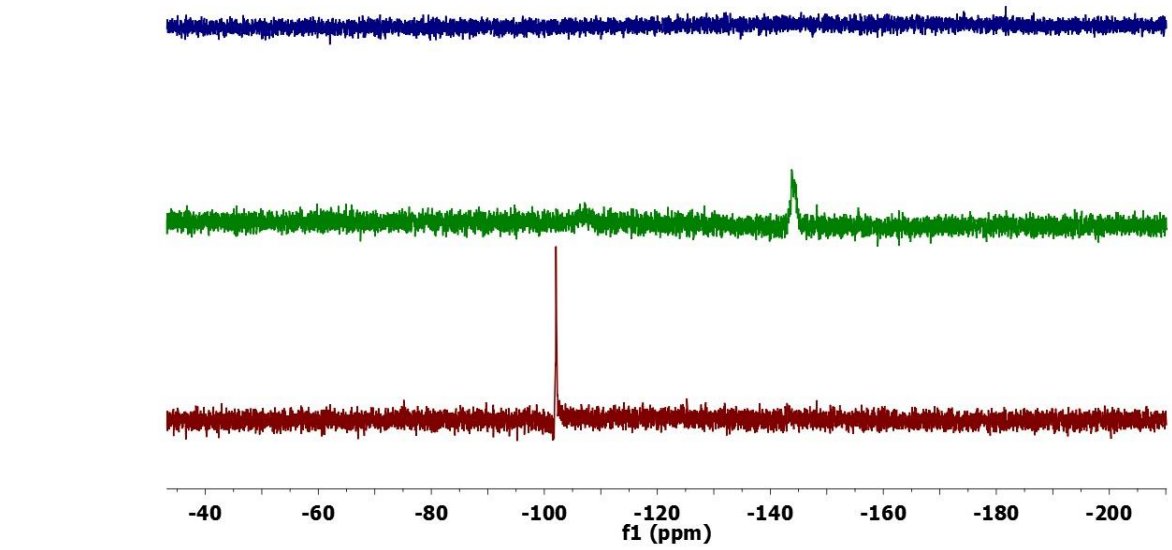

Figure S25: TBAF with **SR1** recorded by ^{19}F NMR spectroscopy (DMSO-d_6, 298 K). **Red**: TBAF solution in DMSO-d_6, **green**: TBAF + **SR1** in DMSO-d_6, **blue**: TBAF + **SR1** + $CuCl_2$ in DMSO/D_2O mixture.

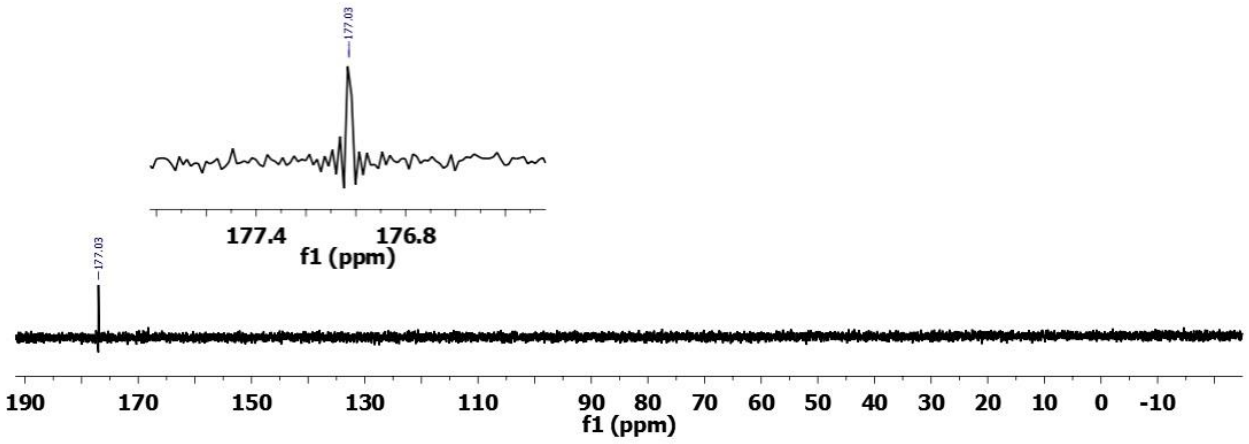

Figure S26: ^{19}F NMR spectrum of the red coloured solution obtained after sequential addition of $CuCl_2$ and TBAF in **SR1** solution in DMSO. Inset: expanded region.

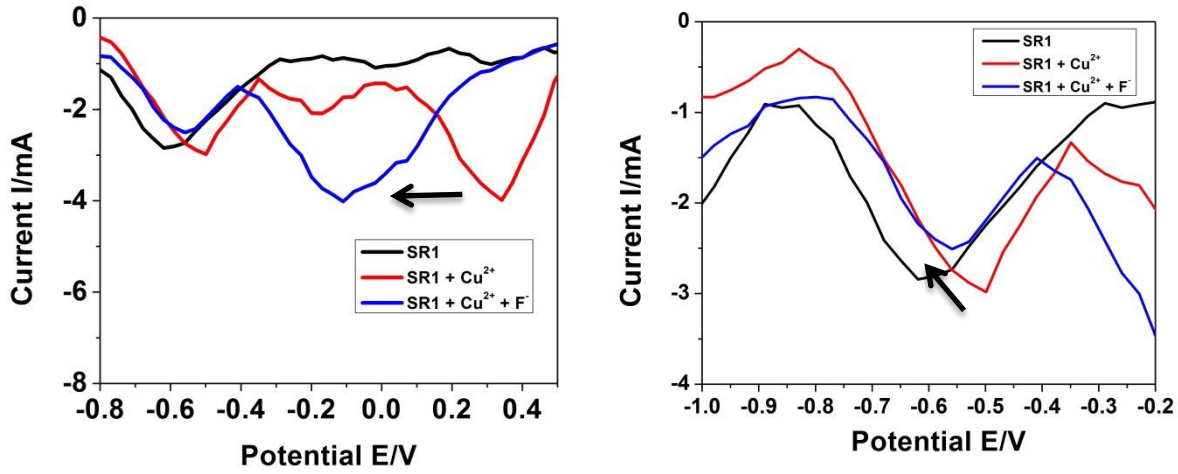

Figure S27: Changes in the DPV (vs Ag/AgCl) curves in presence of n-Bu_4NClO_4 (0.1 M) upon sequential addition of aqueous $CuCl_2$ followed by TBAF solution to a **SR1** solution in DMSO. Left: Changes in the curves w.r.t. the peak corresponding to the Cu^{2+}/Cu^{+} couple; right: Changes in the curves w.r.t. the ligand based peak of **SR1 (Black**: **SR1** solution in DMSO; **red**: **SR1** + $CuCl_2$ in DMSO/water mixture; **blue**: **SR1** + $CuCl_2$ + TBAF in DMSO/water mixture.).

****Note*:** Here particular interest has been laid to the changes in peak at -0.61V vs Ag/AgCl (satd KCl) of ligand (**SR1**) origin **(right)**. A peak corresponding to Cu^{2+}/Cu^{+} couple has also been observed upon addition of aqueous $CuCl_2$ solution at 0.33V which shifts to -0.12V upon addition of fluoride to the aforesaid solution **(left)**. This shift may be ascribed to the increase in concentration of the Cu^{+} ions *w.r.t* concentration of Cu^{2+} and F^{-} species in the bulk solution. The corresponding redox reaction involved in the complexation process is as follows- $Cu^{2+} + 2F^{-} \rightarrow Cu^{+} + F_2$

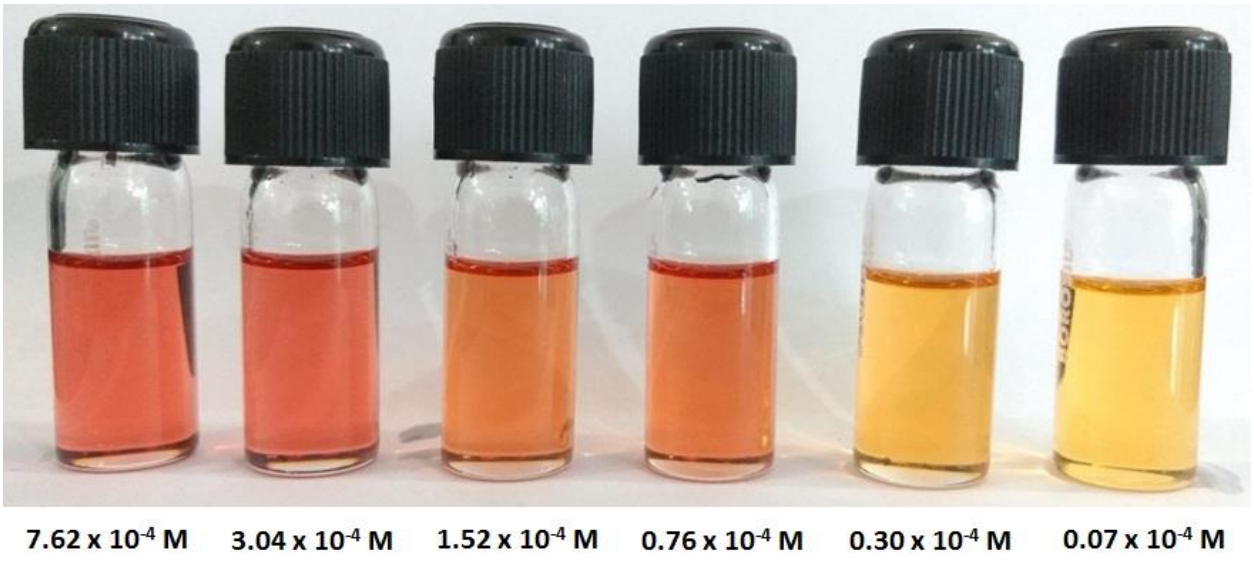

Figure S28: Progressive color change with an increasing amount of aqueous $CuCl_2$ (aq) in the range 0.07 x 10^{-4} M to 7.62 x 10^{-4} M in presence of **SR1 ([SR1] =** 68 x 10^{-6} M**)** and F^- ([F^-] = 15 x 10^{-4} M) in DMSO.

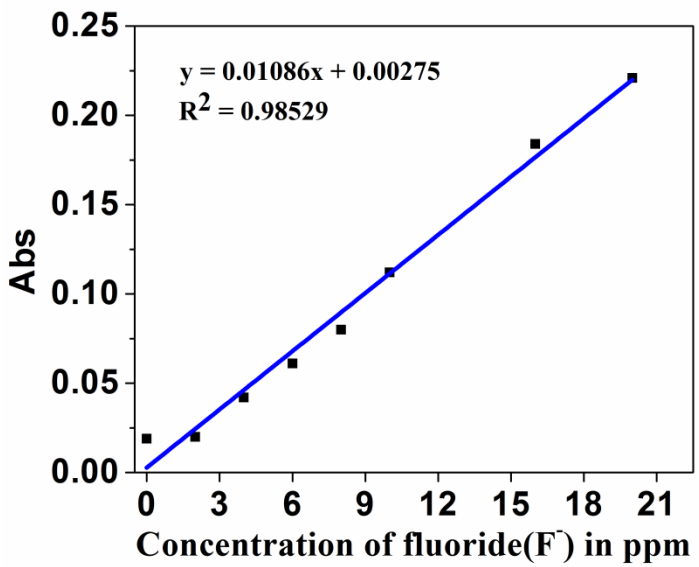

Figure S29: Calibration curve for determining the concentration of fluoride (as TBAF in DMSO) in a sample. [**SR1**] = 68 x 10^{-6} M; [Cu^{2+}] = 15.4 x 10^{-4} M.

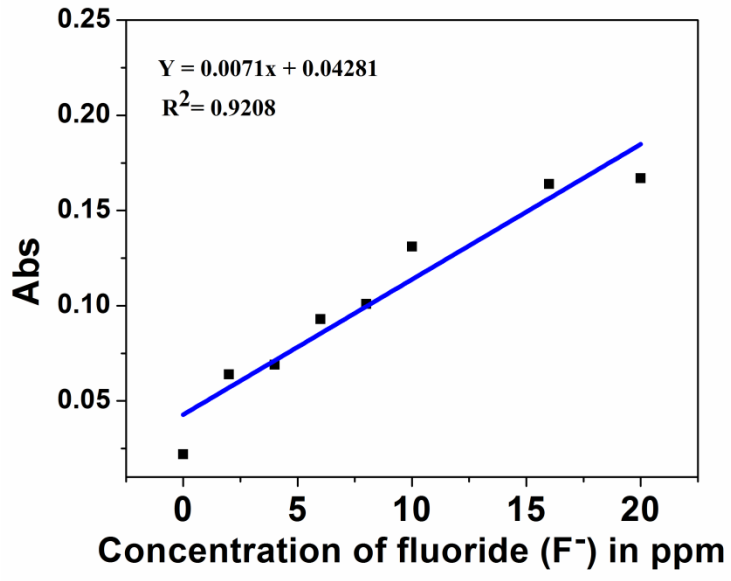

Figure S30: Calibration curve for determining the concentration of fluoride (as NaF in H_2O) in a sample. [**SR1**] = 68 x 10^{-6} M; [Cu^{2+}] = 15.4 x 10^{-5} M

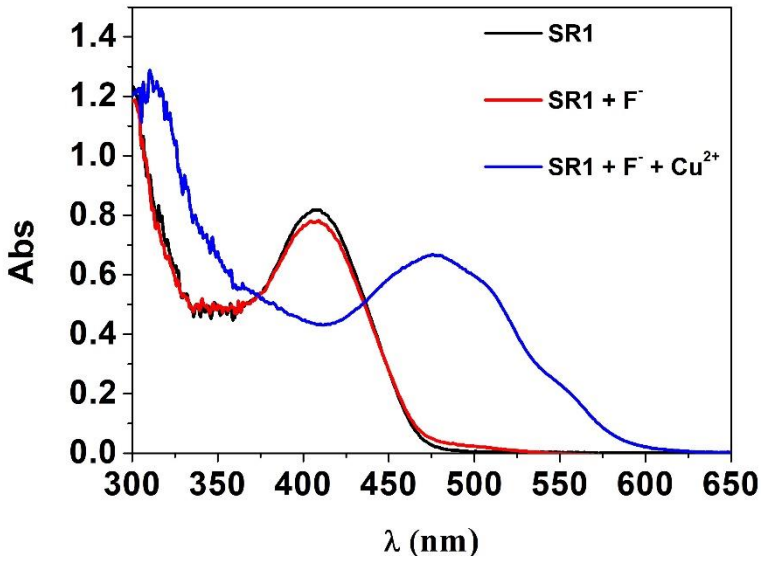

Figure S31: Change in the UV-Vis spectra of **SR1** (**[SR1]** = 68 x 10^{-6} M**)** solution upon addition of aqueous TBAF solution ([F^-]= 61 x 10^{-5} M) followed by aqueous $CuCl_2$ ([Cu^{2+}] = 15.4 x 10^{-5} M) solution.

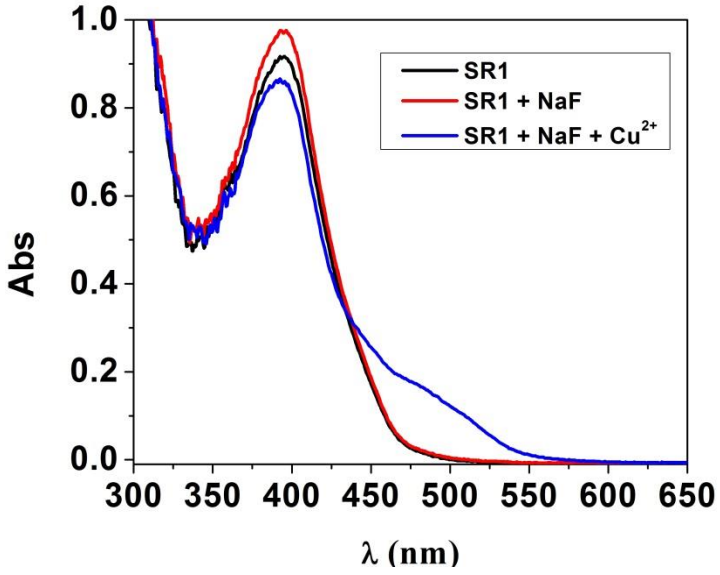

Figure S32: Change in the UV-Vis spectra of **SR1** (**[SR1]** = 68 x 10^{-6} M) solution upon addition of aqueous NaF solution ([F^-] = 1 x 10^{-3} M) followed by aqueous $CuCl_2$ ([Cu^{2+}] = 15.4 x 10^{-5} M) solution.

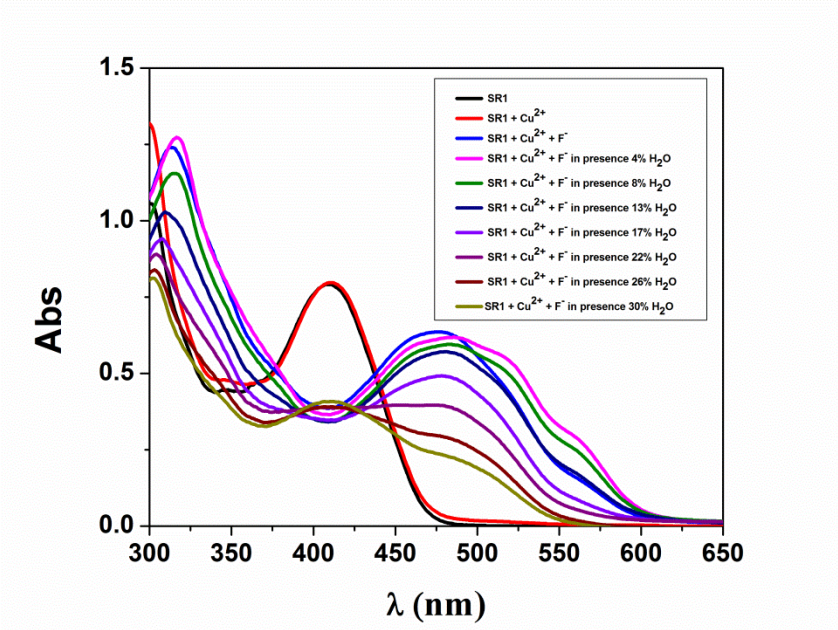

Figure S33: UV-Vis spectra of (**SR1 + Cu^{2+}+ F^-)** red coloured solution after addition of susequent amount of H_2O.

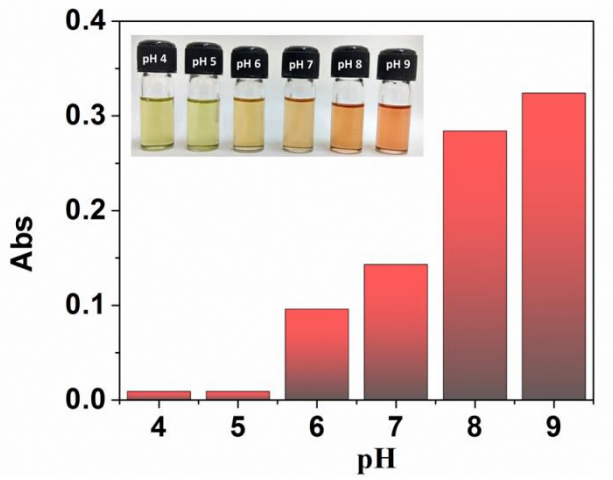

Figure S34: Study on effect of pH on fluoride sensing by **SR1** in presence of aqueous $CuCl_2$ in HEPES buffer (DMSO:Water = 7:3, pH = 7.2).

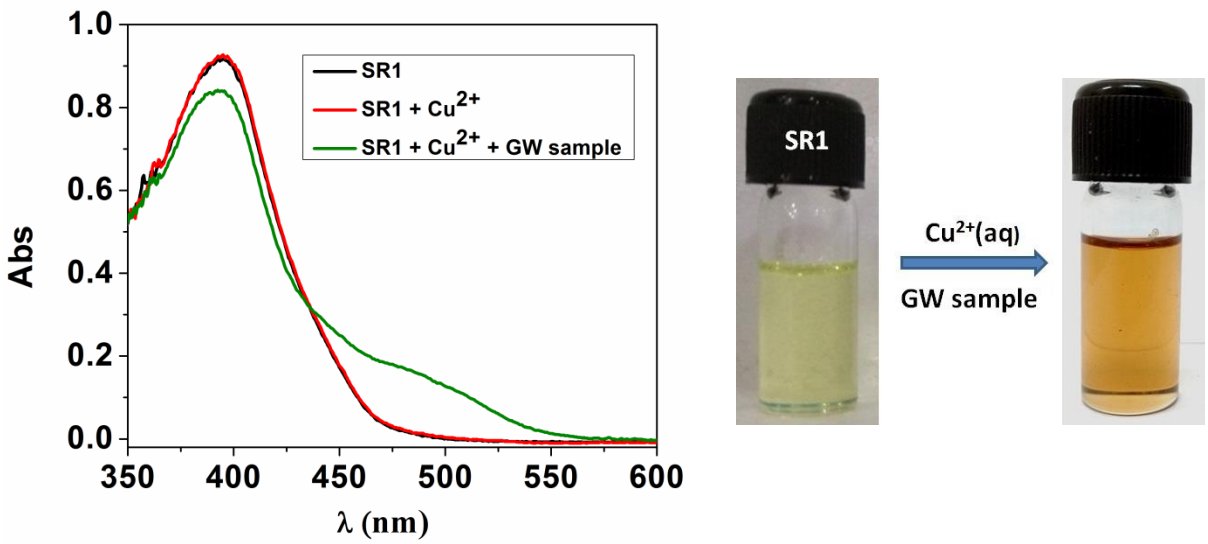

Figure S35: Left: UV-Vis spectra of **SR1** and Cu^{2+} ([**SR1**] = 68 x 10^{-6} M, [Cu^{2+}] = 15.4 x 10^{-5} M) mixture in DMSO/water medium upon addition of ground water (GW) sample (100μL) from fluoride affected area (Baghpani Village, Karbi Anglong district, Assam, India; Coordinates: 26.286372, 93.001249). **Right:** colour change upon sequential addition of $CuCl_2$(aq) and ground water (GW) sample to **SR1** solution in DMSO.

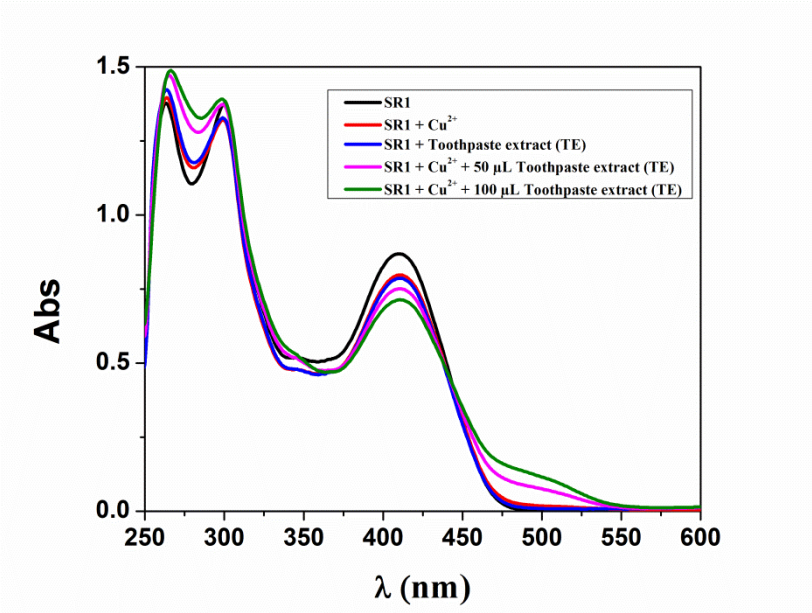

Figure S36: UV-Vis spectra of **SR1** + Cu^{2+} solution after addition of toothpaste solution.

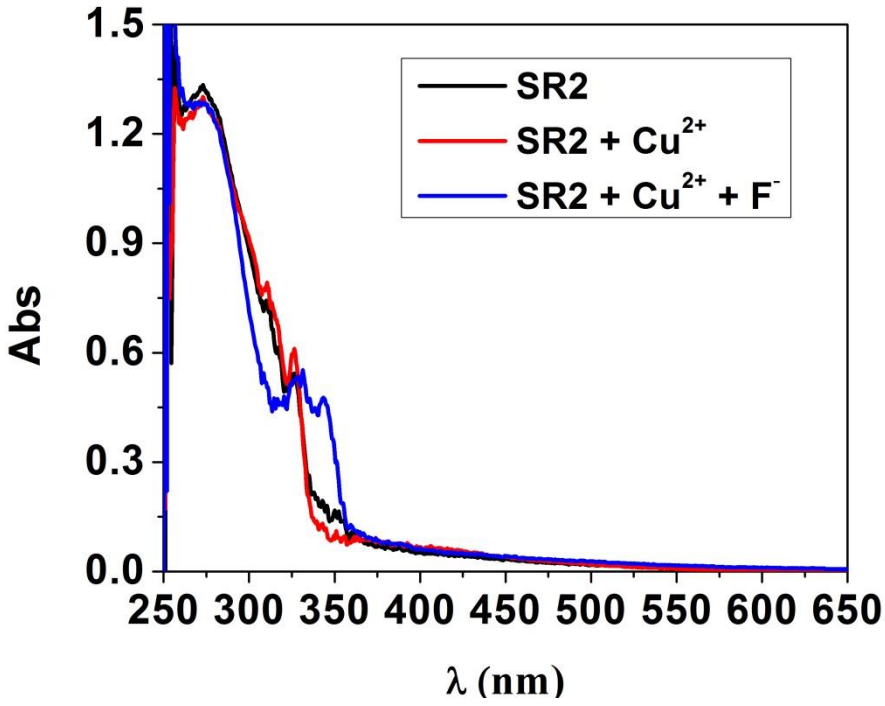

Figure S37: UV-Vis spectra of **SR2** upon sequential addition of aqueous $CuCl_2$ solution followed by F^- in DMSO

Figure S38: Pictorial representation of **SR2** upon sequential addition of aqueous $CuCl_2$ solution followed by F^- in DMSO.

Table S1: Literature reports on fluoride binding study of Dipyrrolylquinoxaline

Receptor system	Salt used for study	Solvent		
		Receptor	**Fluoride**	**Reference**
Dipyrrolylquinoxaline**s**	TBAF	CH_2Cl_2 and DMSO	CH_2Cl_2 and DMSO	*J. Am. Chem. Soc.* 1999, *121*, 10438-10439.
Dipyrrolylquinoxaline	TBAF	CH_2Cl_2	CH_2Cl_2	*J. Am. Chem. Soc.* 2000, *122*, 10268-10272.
Phenanthroline Complexes Bearing Fused Dipyrrolylquinoxaline	TBAF	DMSO	DMSO	*J. Am. Chem. Soc*. 124, 7, 2002, 1134-1135.
dipyrrolylquinoxaline	TBAF	CH_2Cl_2	CH_2Cl_2	*Chem. Commun.*, 2002, 862–863.
Dipyrrolylquinoxaline-Containing Conjugated Polymers	TBAF	CH_2Cl_2	CH_2Cl_2	*Chem. Eur. J.* 2006, 12, 2263 –2269.
Tetrathiafulvalene-annulated dipyrrolylquinoxaline	TBAF	CH_2Cl_2/ CH_3CN (1:1)	CH_2Cl_2/ CH_3CN (1:1)	*Tetrahedron* 2012, 68 (5) 1590-1594.
Poly(methyl methacrylate) copolymers containing dipyrrolylquinoxaline receptors	TBAF	CH_2Cl_2	CH_2Cl_2	*Supramolecular Chemistry* 2011, 24, 101-105.
This Study	TBAF/NaF/toothpaste solution/ Ground water samples	DMSO	H_2O	

Table S2: Literature reports on transition metal based fluoride sensor:

S. No.	Metal receptor system	Fluoride Salt	LOD	Solvent used for study	Ref.
1	copper(II) bis(terpyridine) complex	TBAF	5.07 μM	Acetonitrile	9
2	Co(II) Hexacarboxamide Cryptand Complex	TBAF	2-5 ppm	DMF	10
3	Zn(II) tripodal complex	TBAF/NaF	4.84×10^{-12} M	Water	11
4	2,4-dihydroxybenzaldoxime complex of Cu(II), Ni(II) and Zn(II)	TBAF	4.86 10^{-6} M	DMSO	12
5	Ru(II) complex	TBAF	-	Acetonitrile	13
6	Fe(III) complex	NaF	140 μM	DMSO/Water(3:7)	14
7	Co(II) thiazoline based complex	NaF	-	DMF/water(9:1)	15
8	Zr(IV) EDTA flavonol complex	NaF	3×10^{-6} M	Water	16
9	Zn(II) Terpyridine−Triarylborane Conjugates	TBAF	-	THF	17
10	Ru(II)-bipy based complex	TBAF	1 ppm-10 ppm	Acetonitrile	18
11	amino-naphthoquinone based Co(II), Ni(II), Cu(II), and Zn(II) complexes	TBAF	0.006 μM	DMF/water(3:7)	19
12	Cu(I) Schiff base complex	TBAF/NaF	0.12 μM	DMSO/Water	20
13	**This Study**	**TBAF/NaF**	**0.15 ppm**	**DMSO/Water**	

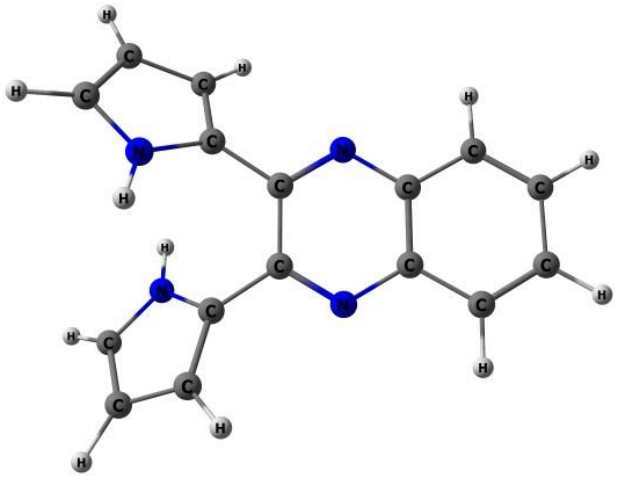

Figure S39: DFT optimized structure of **SR1**.

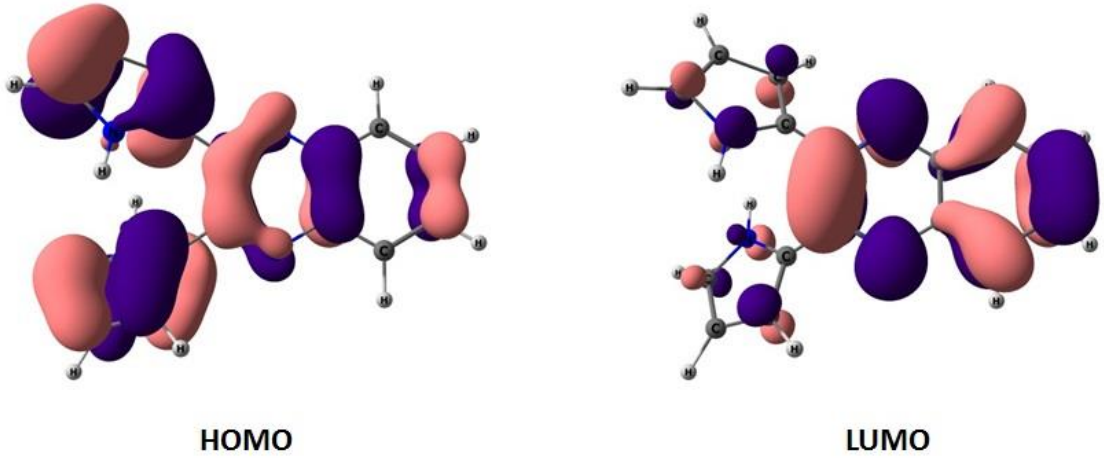

Figure S40: HOMO and LUMO of **SR1**.

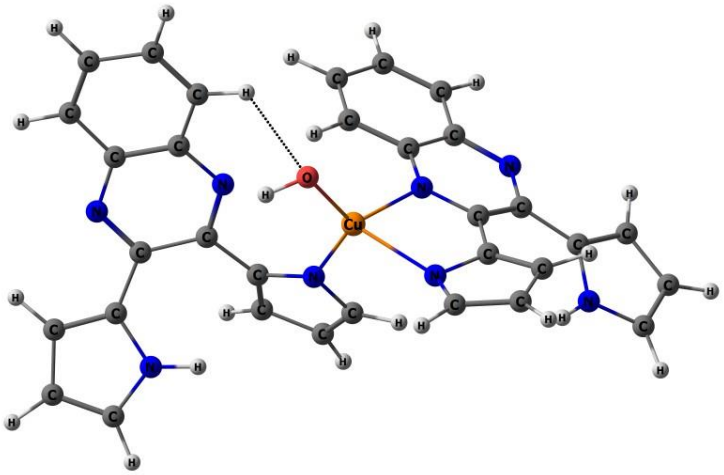

Figure S41: DFT optimized structure of **[Cu(SR1)$_2$OH]$^{2-}$** complex.

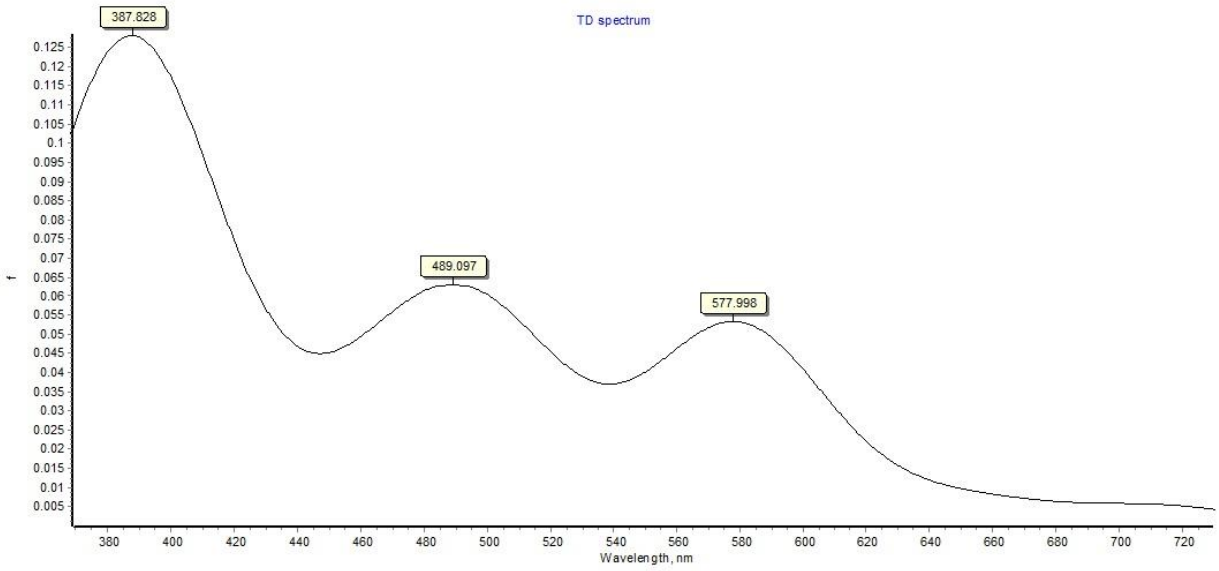

Figure S42: UV-Vis spectrum of **[Cu(SR1)$_2$OH]$^{2-}$** complex simulated from the TD- DFT calculation.

648.1	0.0073
578.98	0.052
572.24	0
513.17	0
508.53	0
501.07	0.0422
490.45	0
486.29	0
477.99	0
477.2	0.0055
473.79	0
468.67	0.0238
457.92	0.0008
426.5	0.0054
398.76	0.0105
385.78	0.1161

Table S3: TD f –values of the obtained UV-Vis spectrum.

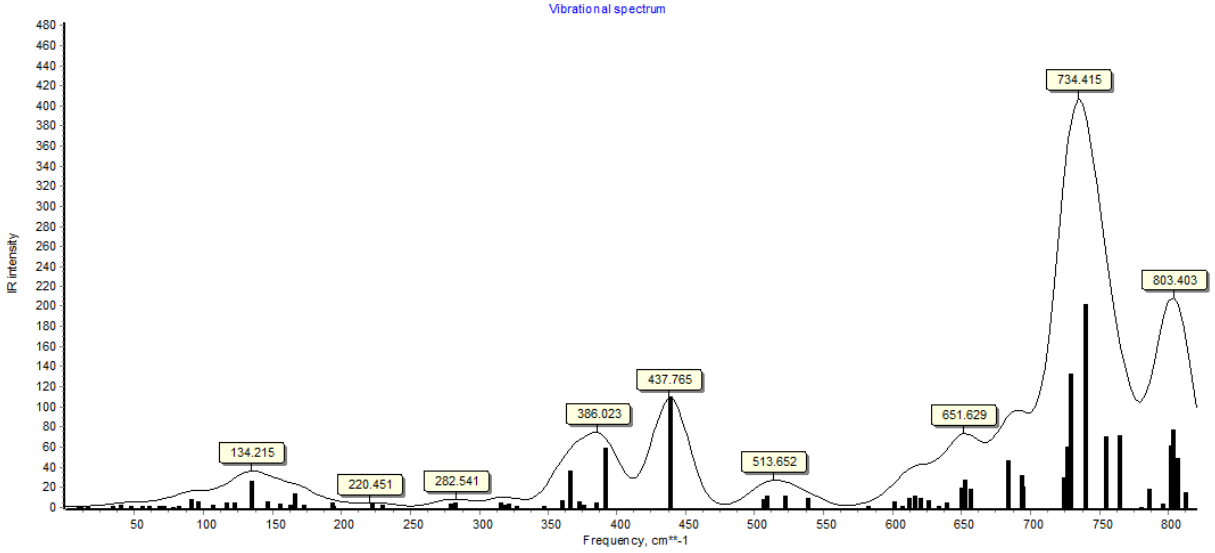

Figure S43: Far-IR spectrum of **$[Cu(SR1)_2OH]^{2-}$** complex found from frequency calculation.

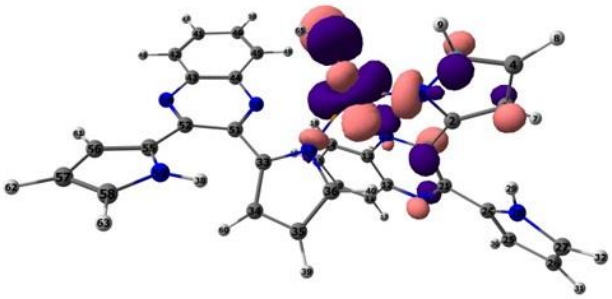

HOMO

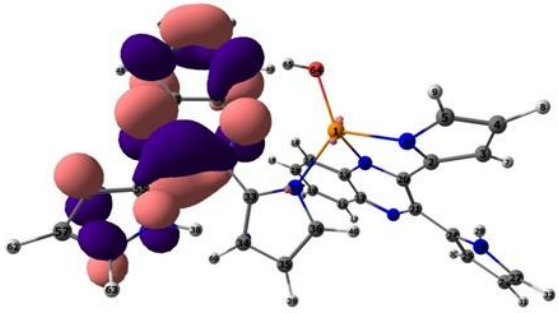

LUMO

Figure S44: HOMO and LUMO of **$[Cu(SR1)_2OH]^{2-}$** complex.

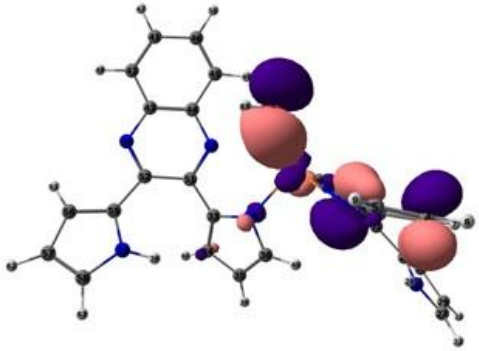

Cu-OH σ-bond (HOMO-8)

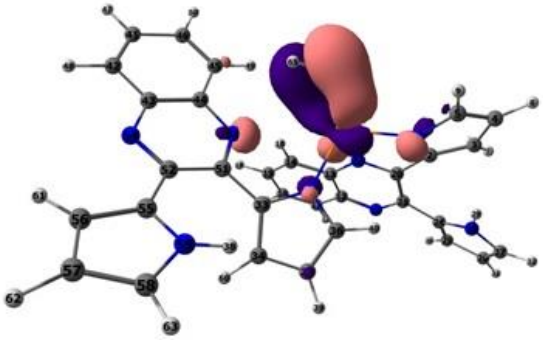

Cu-OH π-bond (HOMO-7)

Figure S45: MOs of the **$[Cu(SR1)_2OH]^{2-}$** complex showing various Cu-OH interactions.

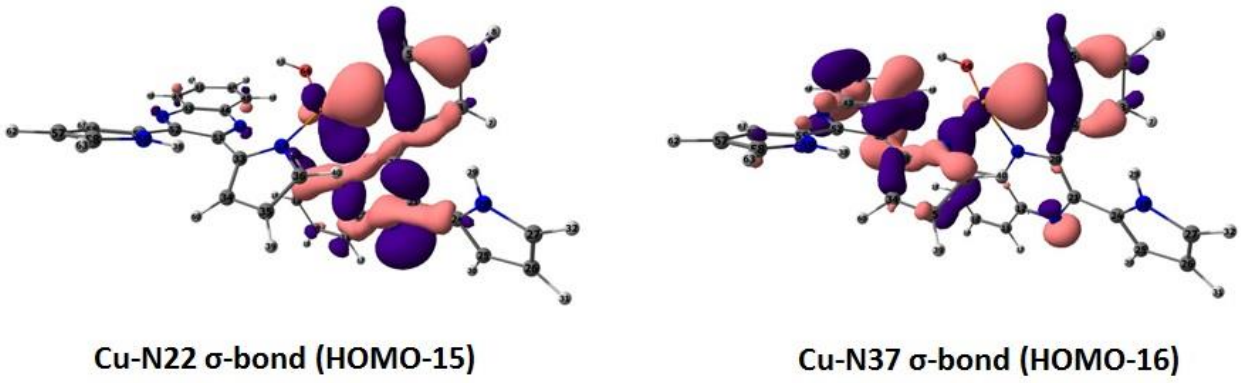

Figure S46: MOs of the **$[Cu(SR1)_2OH]^{2-}$** complex showing various Cu-N interactions.

Table S4: Delocalization energies E(2) for $[Cu(SR1)_2OH]^{2-}$ complex

Donor NBO (i)	Acceptor NBO (j)	E(2) kcal/mol
From unit 1 to unit 2		
88. CR Cu 1	143. LP N 6	0.30
88. CR Cu 1	418. BD* C 5 - N 6	1.03
88. CR Cu 1	430. BD* C 13 - N 22	1.18
88. CR Cu 1	436. BD* C 20 - N 22	1.07
135. LP Cu 1	143. LP N 6	2.66
137. LP Cu 1	143. LP N 6	10.41
137. LP Cu 1	437. BD* C 20 - N 22	11.79
138. LP*Cu 1	433. BD*C 14 - H 18	1.07
From unit 1 to unit 3		
88. CR Cu 1	454. BD*C 33 - N 37	1.25
136. LPCu 1	148. LP N 37	6.54
138. LP*Cu 1	461. BD*C 36 - N 37	1.24
From unit 1 to unit 4		
138. LP*Cu 1	495. BD*O 64 - H 65	1.04
140. LP*Cu 1	495. BD*O 64 - H 65	2.73
From unit 2 to unit 1		
142. LP N 6	138. LP*Cu 1	25.23
142. LP N 6	139. LP*Cu 1	26.63
142. LP N 6	140. LP*Cu 1	3.02
142. LP N 6	141. LP*Cu 1	7.90
144. LP N 22	138. LP*Cu 1	27.89
144. LP N 22	139. LP*Cu 1	5.81
144. LP N 22	140. LP*Cu 1	17.53
144. LP N 22	141. LP*Cu 1	15.63
From unit 3 to unit 1		
147. LP N 37	138. LP*Cu 1	38.08
147. LP N 37	139. LP*Cu 1	11.64

147. LP N 37	140. LP*Cu 1	15.44
From unit 4 to unit 1		
87. BD O 64 - H 65	138. LP*Cu 1	5.25
87. BD O 64 - H 65	139. LP*Cu 1	1.33
87. BD O 64 - H 65	140. LP*Cu 1	8.13
132. CR O 64	138. LP*Cu 1	3.77
132. CR O 64	140. LP*Cu 1	4.69
152. LP O 64	140. LP*Cu 1	13.71
153. LP O 64	141. LP*Cu 1	11.76
154. LP O 64	38. LP*Cu 1	63.21
154. LP O 64	139. LP*Cu 1	0.93
154. LP O 64	140. LP*Cu 1	30.22
From unit 4 to unit 3		
153. LP O 64	477. BD* C 45 - H 49	2.10

Z-matrix of Complex $[Cu(SR1)_2OH]^{2-}$.

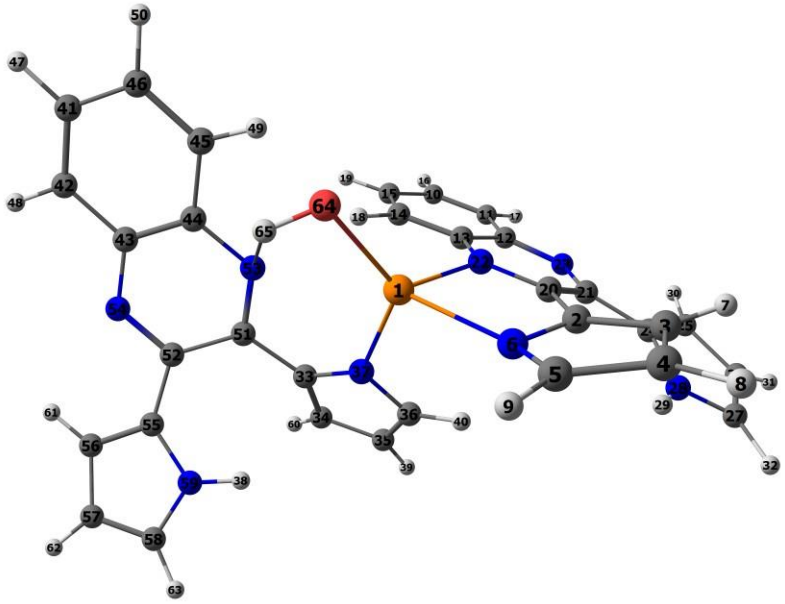

Cu	0.347786000000	0.329329000000	1.445904000000
C	3.269248000000	-0.151068000000	1.674846000000
C	4.409054000000	-0.265419000000	2.521792000000

C	3.927570000000	-0.766325000000	3.757502000000
C	2.528002000000	-0.926070000000	3.601303000000
N	2.127209000000	-0.547399000000	2.357919000000
H	5.416845000000	0.064413000000	2.303902000000
H	4.509693000000	-0.961977000000	4.650111000000
H	1.805782000000	-1.277917000000	4.325486000000
C	1.014637000000	2.952278000000	-3.434891000000
C	2.282276000000	2.429222000000	-3.227981000000
C	2.568041000000	1.711978000000	-2.034505000000
C	1.553909000000	1.563859000000	-1.047011000000
C	0.253405000000	2.084355000000	-1.281502000000
C	-0.007588000000	2.765805000000	-2.458691000000
H	0.790841000000	3.492542000000	-4.351693000000
H	3.074663000000	2.525357000000	-3.963940000000
H	-0.513549000000	1.896798000000	-0.532710000000
H	-1.005798000000	3.153366000000	-2.640669000000
C	3.070236000000	0.419925000000	0.349430000000
C	4.032462000000	0.440683000000	-0.739943000000
N	1.836188000000	0.946531000000	0.153109000000
N	3.799353000000	1.114800000000	-1.871197000000
C	5.297395000000	-0.320972000000	-0.740503000000
C	6.375196000000	-0.203710000000	-1.619826000000
C	7.313485000000	-1.231938000000	-1.296245000000
C	6.777075000000	-1.955663000000	-0.231471000000
N	5.558714000000	-1.400633000000	0.084654000000
H	4.971493000000	-1.632795000000	0.881862000000

H	6.432873000000	0.528324000000	-2.409214000000
H	8.259415000000	-1.424573000000	-1.781653000000
H	7.168562000000	-2.799266000000	0.314848000000
C	-1.575578000000	-1.267043000000	-0.642101000000
C	-1.405619000000	-2.219923000000	-1.685554000000
C	-0.069596000000	-2.680017000000	-1.585671000000
C	0.501406000000	-1.987568000000	-0.492993000000
N	-0.390993000000	-1.123513000000	0.068485000000
H	-2.771587000000	-3.286216000000	-0.389942000000
H	0.427474000000	-3.390889000000	-2.232731000000
H	1.499433000000	-2.073118000000	-0.083523000000
C	-5.495730000000	3.534059000000	0.903869000000
C	-5.829773000000	2.291254000000	0.386431000000
C	-4.807523000000	1.330552000000	0.155552000000
C	-3.452748000000	1.679061000000	0.411557000000
C	-3.125639000000	2.934119000000	0.998633000000
C	-4.140457000000	3.847948000000	1.230678000000
H	-6.273483000000	4.270668000000	1.090283000000
H	-6.856887000000	2.012018000000	0.172912000000
H	-2.086081000000	3.075839000000	1.292569000000
H	-3.910436000000	4.806858000000	1.686300000000
C	-2.725162000000	-0.424137000000	-0.327491000000
C	-4.135164000000	-0.839107000000	-0.404240000000
N	-2.444885000000	0.815589000000	0.079900000000
N	-5.121629000000	0.046985000000	-0.238387000000
C	-4.591167000000	-2.229362000000	-0.584283000000

C	-5.897317000000	-2.683826000000	-0.787044000000
C	-5.864800000000	-4.110809000000	-0.788034000000
C	-4.538335000000	-4.489657000000	-0.577277000000
N	-3.786396000000	-3.347728000000	-0.448944000000
H	-2.128351000000	-2.471229000000	-2.451813000000
H	-6.753049000000	-2.036480000000	-0.891837000000
H	-6.702372000000	-4.779976000000	-0.921114000000
H	-4.086808000000	-5.467276000000	-0.518933000000
O	-0.731125000000	1.522384000000	2.565957000000
H	-1.615565000000	1.118559000000	2.667836000000

Atom No Natural Electron Configuration

Cu 1 [core] 4S (0.29) 3d (9.73) 4p (0.36) 4d (0.02) 5p (0.01)

C 2 [core] 2S (0.85) 2p (3.08) 3p (0.03)

C 3 [core] 2S (0.98) 2p (3.39) 3p (0.02)

C 4 [core] 2S (0.98) 2p (3.36) 3p (0.02)

C 5 [core] 2S (0.93)2p(3.08)3p(0.02)

N 6 [core] 2S (1.40)2p(4.16)3p(0.02)

H 7 1S (0.79)

H 8 1S (0.81)

H 9 1S (0.81)

C 10 [core] 2S (0.97)2p(3.25)3p(0.01)

C 11 [core] 2S (0.97)2p(3.24)3p(0.02)

C 12 [core] 2S (0.85)2p(2.98)3p(0.02)

C 13 [core] 2S (0.85)2p(2.95)3p(0.02)

C 14 [core]2S(0.98)2p(3.18)3p(0.02)

C 15 [core]2S(0.97)2p(3.25)3p(0.01)

H 16 1S(0.80)

H 17 1S(0.78)

H 18 1S(0.73)

H 19 1S(0.79)

C 20 [core]2S(0.85)2p(2.93)3p(0.02)

C 21 [core]2S(0.86)2p(2.92)3p(0.02)

N 22 [core]2S(1.37)2p(4.12)3p(0.02)

N 23 [core]2S(1.39)2p(4.11)3p(0.02)

C 24 [core]2S(0.86)2p(2.98)3p(0.03)

C 25 [core]2S(0.98)2p(3.29)3p(0.01)

C 26 [core]2S(0.98)2p(3.33)3p(0.01)

C 27 [core]2S(0.94)2p(3.09)3p(0.02)

N 28 [core]2S(1.27)2p(4.30)3p(0.01)

H 29 1S(0.53)

H 30 1S(0.77)

H 31 1S(0.80)

H 32 1S(0.80)

C 33 [core]2S(0.84)2p(3.07)3p(0.03)

C 34 [core]2S(0.98)2p(3.38)3p(0.02)

C 35 [core]2S(0.98)2p(3.35)3p(0.02)

C 36 [core]2S(0.94)2p(3.07)3p(0.02)

N 37 [core]2S(1.39)2p(4.17)3p(0.02)

H 38 1S(0.53)

H 39 1S(0.80)

H 40 1S(0.79)

C 41 [core]2S(0.98)2p(3.25)3p(0.01)

C 42 [core]2S(0.97)2p(3.23)3p(0.02)

C 43 [core]2S(0.85)2p(2.98)3p(0.02)

C 44 [core]2S(0.86)2p(2.97)3p(0.02)

C 45 [core]2S(0.99)2p(3.18)3p(0.02)

C 46 [core]2S(0.98)2p(3.25)3p(0.01)

H 47 1S(0.80)

H 48 1S(0.78)

H 49 1S(0.72)

H 50 1S(0.79)

C 51 [core]2S(0.86)2p(2.89)3p(0.02)

C 52 [core]2S(0.87)2p(2.91)3p(0.02)

N 53 [core]2S(1.39)2p(4.06)3p(0.02)

N 54 [core]2S(1.39)2p(4.10)3p(0.02)

C 55 [core]2S(0.86)2p(2.99)3p(0.03)

C 56 [core]2S(0.98)2p(3.28)3p(0.01)

C 57 [core]2S(0.98)2p(3.33)3p(0.01)

C 58 [core]2S(0.94)2p(3.08)3p(0.02)

N 59 [core]2S(1.27)2p(4.29)3p(0.01)

H 60 1S(0.79)

H 61 1S(0.77)

H 62 1S(0.79)

H 63 1S(0.80)

O 64 [core]2S(1.80)2p(5.35)

H 65 1S(0.57)

Z-matrix of the Ligand **SR1**

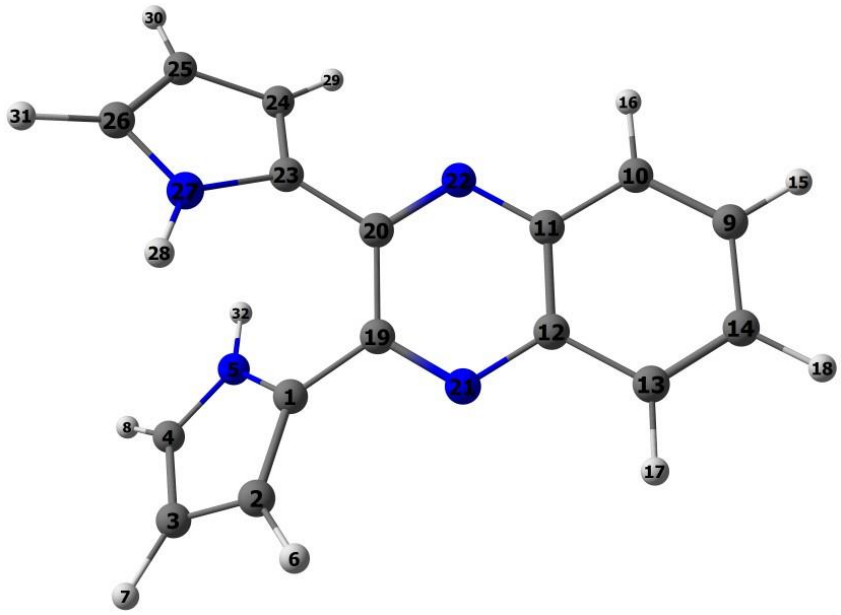

C	1.245401000000	-1.528720000000	0.056725000000
C	1.529877000000	-2.758554000000	-0.529183000000
C	2.827638000000	-3.160066000000	-0.088479000000
C	3.297360000000	-2.170874000000	0.768854000000
N	2.334314000000	-1.187872000000	0.854232000000
H	0.860679000000	-3.294091000000	-1.183478000000
H	3.351029000000	-4.063628000000	-0.357724000000
H	4.224442000000	-2.100641000000	1.314283000000
C	-4.737930000000	0.705599000000	0.106858000000
C	-3.547297000000	1.402490000000	0.207270000000
C	-2.312727000000	0.706481000000	0.096933000000
C	-2.312716000000	-0.706485000000	-0.096930000000
C	-3.547275000000	-1.402515000000	-0.207265000000
C	-4.737919000000	-0.705644000000	-0.106852000000
H	-5.683321000000	1.231334000000	0.185909000000

H	-3.517485000000	2.475624000000	0.355321000000
H	-3.517444000000	-2.475648000000	-0.355324000000
H	-5.683302000000	-1.231394000000	-0.185902000000
C	0.015351000000	-0.728726000000	-0.026704000000
C	0.015339000000	0.728760000000	0.026702000000
N	-1.127900000000	-1.406049000000	-0.126736000000
N	-1.127923000000	1.406062000000	0.126743000000
C	1.245376000000	1.528767000000	-0.056756000000
C	1.529823000000	2.758661000000	0.529043000000
C	2.827632000000	3.160099000000	0.088411000000
C	3.297414000000	2.170802000000	-0.768768000000
N	2.334356000000	1.187810000000	-0.854122000000
H	2.413670000000	0.337209000000	-1.391192000000
H	0.860576000000	3.294288000000	1.183213000000
H	3.351019000000	4.063676000000	0.357612000000
H	4.224543000000	2.100493000000	-1.314105000000
H	2.413577000000	-0.337344000000	1.391425000000

Atom	No	Natural Electron Configuration
C	1	[core]2S(0.85)2p(3.03)3p(0.03)
C	2	[core]2S(0.98)2p(3.26)3p(0.01)
C	3	[core]2S(0.99)2p(3.30)3p(0.01)
C	4	[core]2S(0.95)2p(3.06)3p(0.02)
N	5	[core]2S(1.27)2p(4.31)3p(0.01)
H	6	1S(0.76)

H 7 1S(0.77)

H 8 1S(0.78)

C 9 [core]2S(0.98)2p(3.21)3p(0.01)

C 10 [core]2S(0.98)2p(3.20)3p(0.02)

C 11 [core]2S(0.86)2p(2.97)3p(0.02)

C 12 [core]2S(0.86)2p(2.97)3p(0.02)

C 13 [core]2S(0.98)2p(3.20)3p(0.02)

C 14 [core]2S(0.98)2p(3.21)3p(0.01)

H 15 1S(0.77)

H 16 1S(0.76)

H 17 1S(0.76)

H 18 1S(0.77)

C 19 [core]2S(0.86)2p(2.93)3p(0.02)

C 20 [core]2S(0.86)2p(2.93)3p(0.02)

N 21 [core]2S(1.40)2p(4.05)3p(0.02)

N 22 [core]2S(1.40)2p(4.05)3p(0.02)

C 23 [core]2S(0.85)2p(3.03)3p(0.03)

C 24 [core]2S(0.98)2p(3.26)3p(0.01)

C 25 [core]2S(0.99)2p(3.30)3p(0.01)

C 26 [core]2S(0.95)2p(3.06)3p(0.02)

N 27 [core]2S(1.27)2p(4.31)3p(0.01)

H 28 1S(0.55)

H 29 1S(0.76)

H 30 1S(0.77)

H 31 1S(0.78)

H 32 1S(0.55)

References:

[1] D. A. Armbruster, and T. Pry, *Clin Biochem Rev*, 2008, **29**(Suppl 1), S49-S52.

[2] M.J. Frisch, G.W. Trucks, H.B. Schlegel, G.E. Scuseria, M.A. Robb, J.R. Cheeseman, G. Scalmani, V. Barone, B. Mennucci, G.A. Petersson, H. Nakatsuji, M. Caricato, X. Li, H.P. Hratchian, A.F. Izmaylov, J. Bloino, G. Zheng, J.L. Sonnenberg, M. Hada, M. Ehara, K. Toyota, R. Fukuda, J. Hasegawa, M. Ishida, T. Nakajima, Y. Honda, O. Kitao, H. Nakai, T. Vreven, J.A. Montgomery Jr., J.E. Peralta, F. Ogliaro, M. Bearpark, J.J. Heyd, E. Brothers, K.N. Kudin, V.N. Staroverov, R. Kobayashi, J. Normand, K. Raghavachari, A. Rendell, J.C. Burant, S.S. Iyengar, J. Tomasi, M. Cossi, Rega, N.J. Millam, M. Klene, J.E. Knox, J.B. Cross, V. Bakken, C. Adamo, J. Jaramillo, R.E. Gomperts, O. Stratmann, A.J. Yazyev, R. Austin, C. Cammi, J.W. Pomelli, R. Ochterski, R.L. Martin, K. Morokuma, V.G. Zakrzewski, G.A. Voth, P. Salvador, J.J. Dannenberg, S. Dapprich, A.D. Daniels, O. Farkas, J.B. Foresman, J. V. Ortiz, J. Cioslowski, D.J. Fox, *Gaussian 09, Revision D.01*, Gaussian Inc., Wallingford, CT, 2009.

[3] A. E. Reed, L. A. Curtiss, and F. Weinhold, *Chemical Reviews*, 1988, **88**, 899-926.

[4] J.-D. Chai and M. Head-Gordon, *Phys. Chem. Chem. Phys.*, 2008, **10,** 6615-6620.

[5] M. Dolg, U. Wedig, H. Stoll, and H. Preuss, *J. Chem. Phys.*, 1987, **86**, 866-872.

[6] F. Trani, G. Scalmani, G.S. Zheng, I. Carnimeo, M. J Frisch, V. Barone, *J. Chem. Theory Comput.* 2011, **7**, 3304-3313.

[7] J. L Sessler, H. Maeda, T. Mizuno, V. M. Lynch and H. Furuta, *Chem. Commun.*, 2002, 862-863.

[8] S. P. Mahanta, and P. K. Panda, *J. Chem. Sci*, 2017, **129**, 647-656.

[9] A. K. Purohit, S. K. Padhan, J. R. Mohanty and P. K. Kar, *Photochem. Photobiol. Sci.*, 2018, **17**, 815-821.

[10] J. M. Stauber, G. E. Alliger, D. G. Nocera and C. C. Cummins. *Inorg. Chem.* 2017, **56**, 7615−7619.

[11] J. Singh, M. Yadav, A. Singh and N. Singh, *Dalton Trans.*, 2015, **44**, 12589-12597.

[12] A.Tarai, and J. B. Baruah, *RSC Adv.*, 2015, **5**, 82144-82152.

[13] T. Kundu, A. D. Chowdhury, D. De, S. M. Mobin, V. G. Puranik, A. Datta and G. K. Lahiri, *Dalton Trans.*, 2012, **41**, 4484-4496.

[14] W. Lu, H. Jiang, F. Hu, L. Jiang and Z. Shen, *Tetrahedron*, 2011, **67**, 7909-7912.

[15] J. Wang, H.-B. Liu, W. Wang, Il. Kim and C.-S. Ha, *Dalton Trans.*, 2009, **47**, 10422-10425.

[16] Y. Takahashi, D. A. P. Tanaka, H. Matsunaga and T. M. Suzuki, *J. Chem. Soc., Perkin Trans.* 2, 2002, 759–762.

[17] Y. H. Lee, N. V. Nghia, M. J. Go, J. Lee, S. U. Lee and M. H. Lee, *Organometallics*, 2014, **33**, 753–762.

[18] Z. Lin, Y. Zhao, C. Duan, B. Zhang and Z. Bai, *Dalton Trans.*, 2006, **30**, 3678–3684.

[19] C. Parthiban, S. Ciattini, L. Chelazzi and K. P. Elango, *RSC Adv.*, 2016, **6**, 91265–91274.

[20] R. Das, S. P. Bharati, A. Borborah, P. J. Sarma, B. Das, S. Choudhury, G. Chakrabarty, and S. P. Mahanta. *New J. Chem.*, 2018, **42**, 3758-3764.